

1 Quantifying the Role of Urbanization on Airflow Perturbations and Dunefield Evolution

2 Alexander B. Smith<sup>\*1</sup>, Derek W. T. Jackson<sup>1</sup>, J. Andrew G. Cooper<sup>1,2</sup>, and L. Hernández-

3 Calvento<sup>3</sup>

4 1. School of Geography and Environmental Science, Ulster University, Coleraine, BT52  
5 1SA, Northern Ireland, United Kingdom.

6 2. Geological Sciences, School of Agricultural, Earth and Environmental Sciences,  
7 University of KwaZulu-Natal, Westville Campus, Private Bag X54001, South Africa

8 3. Instituto de Oceanografía y Cambio Global, IOCAG. Universidad de Las Palmas de  
9 Gran Canaria, ULPGC, Parque Científico-Tecnológico de Taliarte, 35214 Telde, Las  
10 Palmas, Spain.

11 Abstract:

12 Rapid urban development has been widespread in many arid regions of the world  
13 during the Anthropocene. Such development has the potential to affect, and be affected by,  
14 local and regional dunefield dynamics. While urban design often includes consideration of  
15 the wind regime, the potential impact of construction on the surrounding environment is  
16 seldom considered and remains poorly understood. In this study regional airflow modelling  
17 during successive stages of urbanization at Maspalomas, Gran Canaria, Spain, indicates  
18 significant and progressive flow perturbations that have altered the adjacent dunefield.  
19 Significant modifications to the boundary layer velocity, mean wind directionality, turbulence  
20 intensity, and sediment flux potential are attributed to the extension of the evolving urban  
21 geometry into the internal boundary layer (IBL).

22 Two distinct process/response zones were identified: (1) the urban shadow zone  
23 where widespread dune stabilization is attributed to the sheltering effect of the urban area on

24 surface wind velocity; and (2) the acceleration zone where airflow is deflected away from the  
25 urbanized area, causing an increase in sediment transport potential and surface erosion.  
26 Consistent coherent turbulent structures were identified at landform and dunefield scales:  
27 counter-rotating vortices develop in the lee-side flow of dune crests and shedding off the  
28 buildings on the downwind edge of the urban area. This study illustrates the direct  
29 geomorphic impact of urbanization on aeolian dunefield dynamics, a relationship that has  
30 received little previous attention. The study provides a template for investigations of the  
31 potential impact of urbanization in arid zones.

32 Keywords: Aeolian dynamics, Anthropogenic impact, Turbulence, Coherent flow structures,  
33 CFD modelling.

## 34 **1. Introduction**

35 Although many natural and anthropogenic factors influence dunefield mobility the  
36 interaction between urbanization and physical processes has been little studied [Nordstrom,  
37 1994; Jackson and Nordstrom, 2011]. The proliferation of urbanization in arid zones during  
38 the past 50 years makes the understanding between human developments and dunefields, a  
39 unique issue of the Anthropocene. Large scale human development of dune environments has  
40 caused a fundamental alteration from a natural state (see review by [Nordstrom, 1994]).  
41 Buildings located adjacent to or within dunefields act as hard impervious structures that  
42 extend into the Internal Boundary Layer (IBL) and impact aeolian dynamics and the regional  
43 geomorphology [Nordstrom and Mcliskey, 1984; Gundlach and Siah, 1987; Nordstrom and  
44 Jackson, 1998]. These small-scale, empirical studies found that buildings invoke airflow  
45 perturbations including steering and changes in wind velocity, and generate secondary flow  
46 patterns (e.g. separation and recirculation cells). These perturbed flow dynamics alter  
47 sediment transport patterns both up- and downwind of buildings [Nordstrom and Mcliskey,

48 1984; Gundlach and Siah, 1987; Nordstrom and Jackson, 1998]. With widespread urban  
49 development in arid regions, the relationship between dunefield dynamics and urban  
50 infrastructure become important considerations. A meso-scale perspective is needed to  
51 provide an understanding of the complexity of regional airflow modified by human  
52 development. Given the difficulties in measuring this influence, numerical models can  
53 provide a broader understanding of impacts at landform and landscape scales.

54 Computational Fluid Dynamics (CFD) has been an increasingly utilized tool for  
55 research in aeolian geomorphology [see review by Smyth, 2016]. It enables the identification  
56 of topographically modified flow including characteristic airflow conditions, complex  
57 turbulent structures [Bauer et al., 2013; Jackson et al., 2013a], and sediment transport patterns  
58 [Lynch et al., 2013; 2016]. Previous CFD studies have identified topographically modified  
59 controls on primary and complex secondary airflow dynamics but none have addressed the  
60 impact of human development (e.g. urbanization) on airflow and dune dynamics. Previous  
61 urban CFD studies have focused on a wide range of issues including airflow and pollutant  
62 dispersion [Murakami et al., 1999; Kim et al., 2003; Pullen et al., 2005; Hanna et al., 2006;  
63 Sabatino et al., 2007; Bai and Park, 2009], building pressures [Richards and Hoxey, 2012],  
64 and human comfort and safety [Blocken et al, 2012; Fadl and Karadelis, 2013]. While these  
65 studies have addressed a wide range of topics they do provide a useful list of methods  
66 addressing model selection, initial boundary conditions, and urban geometries that can be  
67 applied across a range of disciplines.

68 Hernández-Calvento et al. [2014] provided the first study of its kind in implementing  
69 an urban airflow model in a geomorphological context. The authors simulated flow  
70 conditions around the Maspalomas dunefield, Gran Canaria (Spain) using a simplified  
71 numerical model based on a logarithmic wind profile to analyse perturbed flow velocity and  
72 directionality for pre- and post-urbanization of an elevated paleo-alluvial terrace that extends

73 down through the central section of the dunefield. The model surface was tiered using  
74 constant heights for dune topography at 7 m above mean sea level (MSL), the terrace surface  
75 prior to urbanization at 20 m above MSL, and the terrace surface following urbanization at 40  
76 m above MSL. The grid dimensions were 5,000 (x) x 5,000 (y) x 50 (z) with a cell size of 50  
77 m. With this simplified numerical model and idealized terrain surface, significant  
78 perturbations to velocity and steering were identified in relation to simulated ENE wind  
79 conditions. This study implements CFD modelling, on actual dune topography acquired from  
80 LiDAR, and detailed 3D building geometries across the terrace at Maspalomas through time  
81 in order to identify the intensity of regional flow modification at decadal scales.

82 The main objectives of this study are therefore to: (1) identify the regional airflow  
83 perturbations that can be directly attributable to urbanization during various stages of urban  
84 development; (2) describe the geomorphic evolution of the dunefield following each phase of  
85 development; (3) analyse any climatic variability that may have contributed to modified dune  
86 activity through these time periods; (4) determine sediment transport potential and pathways  
87 pre- and post- urbanization; and (5) examine the role of coherent turbulent flow structures  
88 that develop across the dune and urban model surfaces. The study provides a template for  
89 future investigations of actual and potential impacts of urbanization on arid zone dunes.

## 90 **2. Study Site**

91 Maspalomas (27°44'24.73" N and 15°34'26.19" W) is a 3.6 km<sup>2</sup> arid transgressive  
92 dune system located on the southern coast of Gran Canaria, Spain (Fig. 1a,c). The competent  
93 wind regime is bi-modal, characterised by low frequency W storm events and high frequency  
94 prevailing NE trade winds (Fig. 1b). Given the magnitude and frequency of the trade winds,  
95 the dunes migrate from the source area at Playa del Inglés towards the SW to the terminus at

96 Playa de Maspalomas (Fig. 1a). The dunefield is comprised of highly mobile discrete  
97 barchans, barchanoid dune ridges, small parabolics, nebkhas, and sand sheets.

## 98 **2.1. Physical Setting**

99 A narrow offshore shelf, adjacent to Playa del Inglés, provides the majority of  
100 sediment input into the littoral system [Bouzas et al., 2013]. After the sediment moves  
101 through the dunefield, it is redeposited on the offshore shelf at Playa de Maspalomas, the  
102 dunefield acting as a terrestrial sediment conduit. Despite a substantial volume ( $63.1 \times 10^6$   
103  $m^3$ ) of sediment located on the shelf, the system as a whole is in decline as the littoral  
104 deposition of sediment from the NE does not keep pace with the loss of sediment in the SE  
105 [Bouzas et al., 2013]. The updrift shoreline, at Playa del Inglés, has remained relatively  
106 stable in recent decades providing consistent sediment input into the dune system [Fontan et  
107 al., 2012]. The dunefield contains  $18.6 \times 10^6 m^3$  of sediment [Alcántara-Carrió and Fontán,  
108 2009], of which  $14.1 \times 10^6 m^3$  are available for transport [Vallejo et al., 2009]. Hernández et  
109 al. [2007] identified a sediment deficit within the dunefield as the overall heights of the dunes  
110 and accumulation ridges have decreased and the area of deflation down to the basement  
111 alluvium layer has increased over the past 40 years.

## 112 **2.2. Anthropogenic Development**

113 Intense urbanization has occurred across the elevated paleo-alluvial terrace that  
114 extends through the central section of the dunefield, between the mid-1960s until the late  
115 1990s. Prior to the 1960s, this area was primarily agricultural with climbing dunes able to  
116 bypass the terrace before continuing migration unimpeded towards the W [Hernández  
117 Calvento, 2006] (Fig. 2a). By 2006, the terrace was completely urbanized (Fig. 2b). The  
118 margins of the dunefields have also been affected by building of a golf course, apartments,  
119 resorts, hotels and commercial centres. This has led to both a reduction in the aerial extent of

120 the dune field and directly modified the regional sediment pathways and airflow dynamics.  
121 Coinciding with urbanization, the NW section of the dunefield has become widely stabilized  
122 due to the reduction of wind energy, lack of sediment influx, and large scale colonization of  
123 vegetation in this area [Hernández et al., 2007]. In contrast, the active section of the dunefield  
124 has experienced increased erosion as the lowering of the dune topography and the expansion  
125 of deflationary areas has been observed following urban expansion [Hernández et al., 2007].

### 126 **3. Methodology**

127 Here we examine the modified regional airflow patterns during four different stages  
128 of pre- and post- urban development. Case 1 simulates airflow conditions prior to  
129 urbanization. Case 2 simulates flow conditions during the first phase of development in the  
130 mid-1960s and early 1970s. During this period the majority of construction took place at  
131 Maspalomas and initial human perturbation of the airflow occurred. Case 3 represents the  
132 second phase of urbanization where the edges of the terrace were urbanized during the late  
133 1970s and early 1980s. Case 4 represents the last phase of urbanization during the late 1980s  
134 and early 1990s. The most recent buildings were added to the southern extent of the terrace  
135 surface which extends furthest into the central section of the dune field. Aerial photographs  
136 for each stage of urbanization (i.e. Cases 1-4) enable analysis of dunefield response at each  
137 time interval. LiDAR surveys from 2006-2011 illustrate characteristic topographic change in  
138 the dunefield following the last phase of urbanization.

#### 139 **3.1. Dunefield Geomorphology**

140 The geomorphology of the Maspalomas dunefield was examined using historical  
141 aerial photographs from the same time series as the model simulations (i.e. 1961, 1977, 1987,  
142 and 2006). These photographs allow for identification of progressive changes in the total land  
143 cover area of the dunefield, beach, bare sand, deflation, and vegetation surfaces. Dunefield

144 polygons were identified by manually tracing along the low water mark and around the  
145 periphery of dune deposits for each time period. Beach polygons were then extended from the  
146 low water mark to the initial dune deposits inland. The remaining data were classified in  
147 ArcGIS using the iso-cluster unsupervised classification function. Land cover was classified  
148 into three groups (vegetation, deflation or the exposed underlying alluvium layer, and bare  
149 sand areas) based on each classes range of RGB values. These geomorphic classes were then  
150 manually cleaned or amended by overlaying the data on the original photograph to determine  
151 the accuracy of the classification. Vegetation and deflation areas were defined during each  
152 time interval and all other areas within the dunefield (i.e. representing sand sheets, stoss  
153 slopes, slip faces, etc.) were defined as active sand surfaces that are subject to transport.

154 Topographic changes at the dunefield were monitored through successive aerial  
155 LiDAR surveys from 2006, 2008, and 2011. This allows for the quantification of the  
156 topographic and volumetric changes occurring at the study site following the post-  
157 urbanization phase. The 2011 dataset was unfiltered and all data above the sand surface (i.e.  
158 representing vegetation) was removed and considered null within the measurements. Patches  
159 of vegetation were identified in the 2011 survey by running the neighbourhood block  
160 statistics function in ArcGIS to determine the standard deviation of the elevation values  
161 within a 3 x 3 moving window across the DEM surface. Abrupt spikes, representing the  
162 transition between the topography and vegetated areas, were identified from a user defined  
163 threshold as areas exceeding two standard deviations (i.e.  $>0.47$ ) from the mean (i.e. 0.17).  
164 Areas identified as vegetation were then used to mask the 2011 DEM, removing any  
165 overestimation of the bare earth surface in subsequent topographic measurements. By  
166 differencing the model surface we are able to identify key areas of erosion and deposition.  
167 Sediment budgets were then created to determine the net volumetric change of sediment  
168 within the dunefield between each survey interval.

### 169 3.2. Climatic Variability

170 Climatic variability at Maspalomas was analysed for the period 1957 to 2011. Daily  
171 averages of temperature, precipitation and wind speeds were downloaded from the National  
172 Oceanic and Atmospheric Administration (NOAA) National Centers for Environmental  
173 Information (NCEI) database. Regional climatic data were recorded at an Agencia Estatal de  
174 Meteorología (AEMET) station at the Las Palmas de Gran Canaria Airport (LPA) located 25  
175 km northeast of the dunefield. Daily precipitation ( $P$ ) and temperature normals were used to  
176 predict the annual potential evapotranspiration ( $PE$ ) using the Thornthwaite [1948] method at  
177 the study site per annum. Daily averages for wind speed were used to determine the  
178 frequency of winds exceeding the minimum threshold velocity (i.e.  $5.5 \text{ ms}^{-1}$  for the average  
179  $0.22 \text{ mm}$  sediment diameter found within the dunefield; [Bagnold, 1941; Smith et al., 2017])  
180 per year ( $W$ ). Variability in climate was used to determine the dune mobility function ( $M$ ;  
181 Eq. 1) over time to provide an index of climatic controls on dunefield dynamics [Lancaster,  
182 1988].  $M$  values  $< 50$  are considered stable with inactive dunes,  $50-100$  only dune crests are  
183 active,  $100-200$  dunes are active with vegetated interdunes and lower slopes, and  $>200$  dunes  
184 are fully active [Lancaster, 1988].

$$185 \quad M = W/(P:PE) \quad \text{Eq. 1}$$

### 186 3.3. CFD Modelling

187 Modelling of the regional airflow conditions across the study site was conducted in  
188 OpenFOAM, an opensource CFD modelling software. For the simulations conducted in this  
189 study the Re-Normalization Group (RNG)  $k - \varepsilon$  model was implemented because it has  
190 relatively low computational costs and the ability to accurately simulate flow conditions in  
191 complex three dimensional dune environments [Smith et al., 2017]. Atmospheric boundary  
192 layer (ABL) conditions, specified at the model inlet, are free stream velocity ( $U$ ; Eq. 1),



193 turbulent kinetic energy ( $k$ ; Eq. 2), and energy dissipation ( $\varepsilon$ ; Eq. 3) [Richards and Hoxey,  
 194 1993]. Here  $u_*$  represents the shear velocity,  $K$  is von Kármán's constant,  $z$  is the height of  
 195 the reference velocity,  $z_o$  is the aerodynamic roughness length, and  $C_\mu$  is a model constant  
 196 0.09. Initial conditions were taken as the mean wind velocity exceeding threshold conditions  
 197 (i.e.  $7.2 \text{ ms}^{-1}$ ) and taken from highest frequency winds (i.e. ENE) occurring at the site for the  
 198 period of 2006-2013. These ABL conditions were used as the input for all four historical  
 199 models, representing varying stages of urbanization for the years 1961, 1977, 1987, and 2006  
 200 (Fig. 3a).

$$201 \quad U = \frac{u_*}{K} \ln \left( \frac{z+z_o}{z_o} \right) \quad (1)$$

$$202 \quad k = \frac{u_*^2}{\sqrt{C_\mu}} \quad (2)$$

$$203 \quad \varepsilon = \frac{u_*^3}{K(z_o+z)} \quad (3)$$

204 Buildings were modelled within Trimble SketchUp to provide realistic 3D building  
 205 geometries and were overlaid onto the the topographic model surface (Fig. 3a,b). All  
 206 models utilize a LiDAR DEM from 2006 as the characteristic dune topography. Although the  
 207 dunes are highly dynamic, this DEM acts as a model control to look at the direct impact of  
 208 buildings on the regional flow patterns through time without the additional variability due to  
 209 modified bedform-flow interaction. The dunes were designated constant  $z_o$  values of 0.1 m  
 210 [Smith et al., 2017] while the urbanized area was given  $z_o$  values of 0.8 [Troen and Lundtang  
 211 Petersen, 1989]. Jackson and Hunt's [1975] IBL depth (Eq. 4) was used to estimate the  
 212 minimum refinement of the mesh surface in order to reduce computational costs in areas of  
 213 free stream while capturing geomorphically relevant near surface flow conditions. The total  
 214 number of cells within the model domains were  $\sim 2 \times 10^7$  and varies slightly depending on the  
 215 number of buildings added to the model surface (Fig. 3a,b). Surface cell normals are reported

216 at a 1m x 1m resolution; however, cells become increasingly refined (i.e. < 1m x 1m) in areas  
 217 of highly heterogeneous surface slope (e.g. slip faces and building edges) in order to maintain  
 218 an accurate surface gradient. Models were run at a sampling rate of every 0.01 s<sup>-1</sup> and were  
 219 terminated after convergence was achieved when the residuals of the fluctuating model  
 220 components of the 3D flow velocity ( $u, v, w$ ),  $k$ ,  $\varepsilon$ , and surface pressure  $\rho$  all fell below  
 221 0.001.

$$222 \quad \frac{l}{L} \ln\left(\frac{l}{z_0}\right) = 2K^2 \quad (4)$$

223 Model results were measured directly from the model surface including airflow  
 224 direction ( $\theta$ ; Eq. 5), turbulence intensity ( $TI$ ; Eq. 6), and surface shear stress ( $\tau_W$ ; Eq. 7).  
 225 Where  $TKE$  is the turbulent kinetic energy taken as one half of the standard deviation of the  
 226 three flow components (i.e.  $u, v, w$ ),  $U$  is the mean velocity,  $u$  is the horizontal velocity  
 227 parallel to the model surface,  $y$  is the vertical distance to the model wall, and  $\mu$  is the  
 228 molecular dynamic viscosity.

$$229 \quad \theta = \text{atan2}(u, v) \quad (5)$$

$$230 \quad TI = \frac{\sqrt{\frac{2}{3}TKE}}{U} \quad (6)$$

$$231 \quad \tau_W = \mu \frac{\partial u}{\partial y}_{(y=0)} \quad (7)$$

232  $\tau_W$  was used to estimate the potential sediment flux across the entirety of the model  
 233 surface following the techniques developed by [Smith et al., 2017]. Surface shear velocity  
 234 ( $u_*$ ; Eq. 8) was input into Sauermann et al.'s [2001] saturated sediment transport equation  
 235 ( $q_{sat}$ ; Eq. 9). This sediment transport equation acts as potential sediment transport given the  
 236 modified flow velocity at the surface and better estimates intermediate transport conditions

237 where  $u_* \gg u_{*t}$ . This equation has performed well during experiments over barchan dune  
 238 topography and is determined to be a suitable model for the study site [Sauermann et al.,  
 239 2003]. Here  $\rho$  represents the specific weight of air,  $u_{*t}$  is the threshold shear velocity  
 240 [Bagnold, 1941], model constants  $\alpha$  and  $z_1$  [White and Mounla, 1991], the average height of  
 241 saltation  $z_m$  [Owen, 1964], and  $u_{st}$  the minimum velocity of sand grain saltation  
 242 [Sauermann et al., 2001].

$$243 \quad u_* = \sqrt{\left(\frac{\tau_w}{\rho}\right)} \quad (8)$$

$$244 \quad q_{sat} = \begin{cases} 2\alpha \frac{\rho}{g} (u_*^2 - u_{*t}^2) \left( u_* \frac{2}{K} \sqrt{\frac{z_1}{z_m} + \left(1 - \frac{z_1}{z_m}\right) \frac{u_{*t}^2}{u_*^2}} - \frac{2u_{*t}}{K} + u_{st} \right) & \text{for } u_* \geq u_{*t}, \\ 0 & \text{else.} \end{cases} \quad (9)$$

245 Potential sediment transport was corrected using Bagnold's (1973) formula (Eq. 10)  
 246 relative to the localized slope of the surface (G; Eq. 11). Here  $\alpha_r$  is the angle of repose ( $\sim 34^\circ$ )  
 247 and  $\theta_s$  is the local surface slope. For each time series, reported results were normalized to the  
 248 initial pre-urbanization model (i.e.  $t$  and  $\theta_{2,3,4}$ ) using Jackson and Hunt's [1975] fractional  
 249 perturbation ratio for  $q'$  and  $TI$  (Eq. 12).  $\theta$  was normalized to the unperturbed pre-  
 250 urbanization model and is reported as the percent change of flow direction from -50% to  
 251 +50% (Eq. 13).

$$252 \quad q' = G q_{sat} \quad (10)$$

$$253 \quad G = \frac{\tan \alpha_r}{\cos \theta_s (\tan \alpha_r + \tan \theta_s)} \quad (11)$$

$$254 \quad \delta_{(q', TI)} = \frac{t_{(2,3,4)} - t_1}{t_1} \quad (12)$$

$$255 \quad \Delta_\theta = \frac{\theta_{(2,3,4)} - \theta_1}{360} \quad (13)$$

## 256 4. Results

### 257 4.1. Land Cover and Topographic Change

258 The physical extent of the Maspalomas dunefield has been reduced by 17% between  
259 1961 and 2006 (Fig. 4; Table 1). Agricultural encroachment of the dunefield was already  
260 occurring prior to 1961; however, the majority of the reduction is due to large scale urban  
261 development during the mid-1960s (Fig 4a,b; Table 1). During subsequent construction  
262 phases between the 1970s and 1990s the entire southern terrace was urbanized, cutting off the  
263 sediment supply to the northwest section of the dunefield (Fig. 4c,d). During this 50 year  
264 period three distinct morphological trends are evident in the boundaries of the dunefield: a) a  
265 retrograding coastline at Playa de Maspalomas; b) episodic pro- and retro- grading coastline  
266 at Cape La Bajeta; and c) stability of the coastline at Playa del Inglés (Fig. 4).

267 Within the dunefield, large scale land cover changes have been observed at the  
268 decadal scale. Bare sand surfaces were reduced by 34% between 1961 and 2006 (Fig 4; Table  
269 1) concomitant with increases of 310% and 145%, respectively in the surface coverage of  
270 vegetated and deflation areas. In the active dune area the interdune spacing has increased,  
271 evident in continual expansion of deflation areas between dune deposits, particularly adjacent  
272 to the source area at Playa del Inglés. Beach area has nearly doubled during the study time  
273 period. This is largely attributed to the increased width of Playa del Inglés. The intermittent  
274 foredune in the NE section has been stabilized by vegetation over the past twenty years  
275 [Hernández Calvento, 2006]; however, in the E/SE extent the development of incipient  
276 barchan dunes and barchanoid dune ridges is occurring at increasingly further distances  
277 downwind of the sediment source area (Fig. 4).

278 Topographic changes, measured from repeat aerial LiDAR surveys, indicate a net  
279 sediment loss from the Maspalomas dunefield from 2006 to 2011 (Fig. 5a,b). Between 2006

280 and 2008 234,676 m<sup>3</sup> was lost, primarily from the active section of the dunefield (Fig 5a).  
281 Across the northwest section the surface has become highly stabilized and shows only small  
282 topographic changes. Similar net sediment loss occurred between 2008 and 2011 when  
283 315,171 m<sup>3</sup> was removed from the dunefield (Fig. 5b). At Playa de Maspalomas the  
284 retrograding coastline is encroaching on the dunes in the southwest section of the dunefield  
285 with a retreat of up to ~106 m between 1961 and 2006. Migrating dunes show a general trend  
286 of reduction in crest height through time. In total the system displays a high level of  
287 sediment deficit. At the current rate of net erosion (~110,000 m<sup>3</sup> per year), the 14.1 x 10<sup>6</sup> m<sup>3</sup>  
288 of active sediment [Vallejo et al., 2009] could be depleted within ~128 years.

## 289 4.2. Climatic Controls

290 Low precipitation, warm temperatures, and high wind energy promote high dune  
291 activity at Maspalomas. Mobility index values 1957- 2011 (Fig. 6) show the dunes to be fully  
292 active (i.e.  $M > 200$ ) except during 1957 and 1962 (i.e.  $100 < M < 200$ ). Wind speeds are  
293 unavailable for 1963-1964 and 1967-1972. Spikes in  $M$  show that certain years have  
294 increased erosive potential. The largest  $M$  occurs in 1961 when the dune field experienced  
295 hyper-arid conditions (i.e.  $P:PE < .05$ ; [UNCCD, 1994]). Other years recording hyper-arid  
296 conditions were 1961, 1963, 1975, 1976, and 1977. All other years recorded arid conditions  
297 (i.e.  $0.05 - 0.20$ ) except for 1971, 1972, 1989, 1991, 1993, and 2005 which recorded semi-  
298 arid conditions (i.e.  $P:PE < 0.20-0.50$ ). Fluctuations in aridity have the most direct impact  
299 on  $M$  at Maspalomas.  $W$  remains relatively consistent with an average of 62% of days per  
300 year exceeding threshold conditions. There is a slight overall decline in  $M$  due to the decrease  
301 in drought conditions experienced in the 1960s and 1970s; however,  $M$  values have remained  
302 relatively high with the potential to promote the development of fully active dunes with  
303 limited influence of vegetation stabilizing the surface.

### 304 4.3. Regional Airflow and Sediment Transport Dynamics

305 The initial ABL conditions designated at the CFD domain inlet were specified for  
306 each model as  $U = 7.2 \text{ ms}^{-1}$ ,  $u_* = 0.67 \text{ ms}^{-1}$ ,  $k = 1.52 \text{ m}^2\text{s}^{-2}$ ,  $\theta = 72^\circ$ ,  $\varepsilon = 0.07 \text{ m}^2\text{s}^{-3}$ , and  $\rho = 0$   
307  $\text{m}^2\text{s}^{-2}$ . The only variability in model simulations occurs when adding the representative  
308 building geometries through time during Case 2 (1977), Case 3 (1987), and Case 4 (2006).  
309 This allows direct comparison of the influence of the different stages of urban construction on  
310 the magnitude of regional airflow perturbations, relative to the pre-urbanized airflow  
311 conditions represented by Case 1 (1961).

#### 312 4.3.1. Sediment Flux Potential

313 Prior to urbanization airflow transitions from the open sea and a relatively flat beach  
314 face before acceleration occurs over the accumulation zones in the central section of the  
315 dunefield. Here, airflow is compressed and accelerates over elevated barchanoid dune ridges  
316 and the alluvial terrace surface leading to higher rates of predicted  $q'$  (Fig. 7a). Downwind of  
317 the terrace and large barchanoid ridges, there is a natural reduction in  $q'$  as energy is  
318 dissipated following IBL flow over elevated bedforms with increasing surface roughness  
319 (Fig. 6a). During case 2 (Fig. 6b), much of the surface to the E and S of the terrace  
320 experiences an increase of  $0.20 - 0.40 \delta q'$  as airflow is modified by the building geometries.  
321 The largest increase ( $>0.40$ ) occurs at the dunes on the boundary of the terrace. Reduction in  
322  $\delta q'$  is observed downwind with ranges of values of  $<-0.80$  in the immediate boundary  
323 between the urban terrace declining to  $-0.40 - -0.20$  at  $\sim 500\text{m}$  downwind and  $>-0.20$  at the  
324 W/NW extent of the dunefield (Fig. 7b). Detached flow conditions downwind of the urban  
325 terrace do not have sufficient length to reach flow recovery within the shadow zone causing a  
326 reduction in  $\delta q'$  across the entire NW sector of the dunefield.

327

328 Case 3 shows similar results as Case 2, however, the magnitude of surface flow  
329 velocity perturbations has increased (Fig. 7c). There is an increase of  $\delta q'$  between 0.60 –  
330 0.80 of surface velocity around the urban-dunefield margin at the S end of the terrace.  
331 Elevated  $\delta q'$  predictions continue towards the southwest of the terrace across barchan dune  
332 ridges with an increase of 0.20 – 0.40. At Playa de Maspalomas,  $\delta q'$  is less magnified with  
333 an increase of up to 0.10 – 0.20 except for the uppermost dune crests which still record an  
334 increase of  $\delta q'$  up to 0.20 – 0.40. The deceleration of flow in the urban shadow zone is  
335 further magnified during Case 3, with much of the surface area experiencing a decrease in  
336  $\delta q'$  between -0.40 - -0.20 (Fig. 7c). This area of retarded  $\delta q'$  extends further downwind  
337 ~1km from the edge of the urban terrace. Further changes to  $\delta q'$  in Case 4 are only slightly  
338 modified in comparison to Case 3. The largest  $\delta q'$  perturbations are manifest in the  
339 acceleration of flow E and S of the terrace. Here the buildings built during the last  
340 construction phase are relatively high and create an amplified localized impact on the  
341 regional flow patterns. The dunes near this section of the terrace experience an increase in  
342  $\delta q'$  of over 0.80 greater than pre-urbanization conditions (Fig. 7d). Overall, the rest of the  
343 dunefield displays similar results to cases 2 and 3 with magnified  $\delta q'$  across much of the  
344 active dune surface and a subsequent reduction of  $\delta q'$  across the majority of the NW section  
345 of the dunefield. The first two phases of construction (i.e. Case 2 and 3) had the largest  
346 impact on  $\delta q'$  causing significant modification of dunefield sediment dynamics in response  
347 to urbanization (Fig. 7b,c), with only slight additional modifications occurring following the  
348 final phase (i.e. Case 4).

#### 349 **4.3.2. Surface flow direction**

350 Prior to urbanization  $\theta$  is relatively unperturbed with ENE winds veering slightly  
351 towards the NE across much of the active dune surface. Directly downwind of the alluvial

352 terrace, short recirculation cells develop as airflow is detached from the elevated terrace  
353 surface and recirculated towards the W base of the terrace (Fig 8a). During Case 2,  
354 approaching airflow is shifted slightly to more northerly winds across most of the dunefield.  
355 The largest  $\Delta\theta$  is recorded across the active section of the dunefield, SW of the terrace  
356 surface, with flow being deflected  $\sim 12^\circ$  towards more northerly winds compared to  
357 unperturbed flow conditions prior to urbanization. Across the urbanized surface, the  $\Delta\theta$   
358 across the buildings, inter-building (i.e. streets and parks), and downwind of the terrace are  
359 greatly modified (Fig 8b). Recirculation cells with increased lengths ( $\sim 125$  m) begin to  
360 develop in response to buildings being added to the W surface of the terrace.

361 Case 3 displays larger magnitudes of  $\Delta\theta$  with winds being shifted up to  $12^\circ$  northerly  
362 as airflow approaches the windward side of the terrace and  $12^\circ$  easterly downwind of the  
363 terrace (Fig. 8c). Airflow on the windward side of the terrace is being redirected towards the  
364 southwest before flow begins to shift towards the west as airflow moves around the terrace.  
365 This suggests that airflow is being compressed and redirected before expansion occurs  
366 downwind of the terrace as flow conditions begins to normalise. In the immediate lee of the  
367 urban terrace, large scale recirculation cells are developed with flow being recirculated up to  
368  $162^\circ$  from the unperturbed surface directions. Case 4 displays similar patterns, however, the  
369 magnitude of  $\Delta\theta$  is again increased. The dune ridges to the E of the terrace experience  
370 northerly flow deflection of  $\sim 25^\circ$  (Fig 8d). As airflow moves around the terrace a  $\sim 21^\circ$   
371 easterly deflection of winds occurs across the western section of the dunefield. The  
372 recirculation cells increase in length by  $>200$  m downwind of the prominent buildings added  
373 in the last phase of urbanization. Each phase of construction had a significant impact on  $\Delta\theta$ ;  
374 however, the intensity of steering increased the most during Cases 3 and 4.

### 375 4.3.3 Surface Turbulence Intensity



376 Case 1 displays a surface with  $TI$  values largely between 1.25-1.75, with elevated  
377 values occurring in the lee of higher dune crests in the central section of the dune field and  
378 downwind of the alluvial terrace (Fig. 9a). Subsequent cases show an increase in  $\delta TI$  values  
379 across the urbanized terrace, in the lee of the dune crests, and interdune areas while  
380 displaying a drop in  $\delta TI$  across the stoss slopes. This acceleration across the stoss slopes  
381 reduces  $\delta TI$  values, where sediment flux is usually controlled by the generation of  
382 streamwise stress as airflow accelerates towards the crest. As flow detachment occurs at the  
383 crest, highly turbulent flow conditions transfer momentum towards the surface from the  
384 overlying wake zone causing increase in  $TI$ . This leads to intermittent erosive potential due to  
385 turbulent forces that are not accounted for in the  $q'$  estimates. Increase in  $\delta TI$  can also  
386 potentially lead to increased dune spacing as sediment is being either recycled back towards  
387 the lee slope base in response to recirculating vortices or further downwind to the next dune  
388 deposit as the IBL begins to normalize beyond the point of reattachment [Walker and  
389 Nickling, 2002; Baddock et al., 2007].

390 Highly turbulent coherent flow structures, in the form of two counter-rotating  
391 vortices, are identified across much of the dune topography that experiences recirculating  
392 secondary airflow patterns. These correspond with elevated  $TI$  and  $\delta TI$  in the lee-side  
393 locations, indicated in red (Fig. 9a,b,c,d). The ubiquity of these features across much of the  
394 dunefield surface suggests they have a significant influence on dune spacing. Elevated  $\delta TI$  is  
395 recorded in many lee slope and interdune surfaces following urbanization, potentially  
396 accelerating the erosive potential in low velocity environments.  $\delta TI$  is largely modified  
397 following the initial construction phase, represented in Case 2, with subsequent Cases (i.e. 3  
398 and 4) showing only a slight increase in  $\delta TI$  magnitude. The shadow zone also displays  
399 elevated  $\delta TI$  values following urbanization (Fig. 9b,c,d). Bare sand deposits, not stabilized  
400 by the sheltering effect of vegetation, have the potential to be reworked despite the drop in  $q'$ .

401 This corresponds well with the observed topographic changes showing areas of both low  
402 magnitude erosion and deposition. Given the limitations of the influx of new sediment to this  
403 region, all topographic changes are assumed to involve redistribution of pre-existing deposits.  
404 Progressive construction phases display an increase in  $\delta TI$  magnitude and length downwind  
405 of the terrace, displaying the progressively intensified turbulent nature of flow over the urban  
406 area.

## 407 **5. Discussion**

408 Since urbanization of the alluvial terrace at Maspalomas began during the mid-1960s  
409 there has been clear dichotomy of geomorphic evolution of the dunefield. In the urban  
410 shadow zone, large scale stabilization is manifest in an exponential increase of vegetation that  
411 anchors existing dune forms. Redistribution of sediment occurs over the pre-existing bare  
412 sand deposits and deflation areas. In contrast, the acceleration zone has seen increased  
413 sediment transport due to increased velocity of airflow across the active dune surfaces.  
414 Increased  $\delta q'$  has led to the overall lowering of the dune crests and increase in deflation areas  
415 as the erosive potential exceeds sediment input into the system. Although there has been a  
416 reduction of predicted  $M$  through time (Fig. 6), it is clear that the controls on dunefield  
417 dynamics, defined by Kocurek and Lancaster [1999], have been significantly altered by urban  
418 development. The authors proposed an 'Aeolian System Sediment State' model that suggests  
419 dunefields are controlled by three over-arching variables: sediment supply, susceptibility of  
420 sediment to be transported, and the competence of the local wind regime. In this context, our  
421 study site displays a sediment supply that has remained relatively constant with the source  
422 area at Playa del Ingles experiencing equilibrium over the last 50 years; however, the urban  
423 shadow zone has been directly cut off from new sediment inputs by urban development  
424 starving the northwest sector of new sediment influx. The susceptibility of sediment to  
425 transport has decreased due to both the increase in vegetation in the urban shadow zone and

426 deflation areas in the acceleration zone. This is directly linked to the reduction of bare sand  
427 surfaces available for sediment transport and is characteristic of a dune system that is in  
428 decline. Lastly, there has been a decrease of the competent wind regime downwind of the  
429 urban area and an increase in airflow competence in the active section of the dunefield  
430 promoting both retarded and elevated rates of erosion in both respective regions of the  
431 dunefield.

432         The dynamism of dunefield evolution has often been linked to fluctuations in climatic  
433 variables including  $W$ ,  $P$ , and  $PE$  [Lancaster, 1987; Muhs and Maat, 1993; Wiggs et al.,  
434 1995; Stetler and Gaylord, 1996; Wolfe, 1996; Bullard et al., 1997; Lancaster, 1997;  
435 Lancaster and Helm, 2000; Muhs et al., 2003; Hugenholtz and Wolfe, 2005; Thomas et al.,  
436 2005]. At the dunefield scale, it is unusual to find accelerated or re-activated transport and  
437 stabilization during the same climatic conditions. Simultaneous dunefield stabilization and  
438 increased mobilization have been identified in the Negev-Sinai desert and the coastal sand  
439 dunes in Ceará State in Northeast Brazil [Yizhaq et al., 2007; Tsoar et al., 2009]. In the Ceará  
440 State dunefield, this was attributed to the seasonality of strong wind conditions that can lead  
441 to the degradation of vegetation in spatially limited areas causing the reactivation of the  
442 underlying sediment. In the Negev-Sinai desert, variability in dunefield mobility is due to  
443 human land use differences on the Egyptian (grazing and gathering) and Israeli (inactive)  
444 sides [Meir and Tsoar, 1996; Yizhaq et al., 2007]. While these studies provide evidence that  
445 both climatic and human impacts have an effect on the mobility of dunefields, they are still  
446 relatively limited because they do not account for the perturbations of IBL flow conditions as  
447 a result of dune topography or other regional controls [Bullard et al., 1997]. Our work shows  
448 that urbanization, adjacent to dunefields, can have a direct impact on IBL airflow and can  
449 significantly alter regional airflow dynamics and geomorphic evolution at the dune and  
450 dunefield scale.

451 Hernández-Calvento et al. [2014] conducted the first model to analyse the impact of  
452 urbanization on the regional airflow perturbations across a dunefield. Here we build upon this  
453 original study by providing a coupled meso-scale CFD model using detailed building  
454 geometries and actual dune topography. The perturbations of regional airflow from  
455 urbanization development and associated impacts on a natural dunefield systems has  
456 provided highly detailed information on actual modifications of sediment flux potential,  
457 directionality, and *TI*. These modified flow patterns have had a deterministic impact on the  
458 geomorphology of the dune system and has led to both the simultaneous stabilization and  
459 acceleration of erosion within the dunefield. This has fundamentally transformed the system  
460 at the decadal scale to adjacent areas of highly stabilized and increasingly activated dune  
461 dynamics, overriding limited fluctuations in climatic variability.

## 462 **5.1. Land Cover and Topographic Change**

463 Despite the negative sediment budget of the dunefield and marine deposits [MMA,  
464 2007; Bouzas et al., 2013], there has been an equilibrium of the dune system source area  
465 deposits at Playa del Inglés over the past 50 years [Fontan et al.,2012; Quevedo Medina and  
466 Hernández-Calvento, 2014]. This suggests a relatively consistent supply of sediment at the  
467 decadal scale. At this same temporal scale, urbanization on the alluvial terrace and NW edge  
468 of the dunefield has directly reduced the areal extent of the dunefield (Fig 4). Further  
469 reduction of the dunefield area is also evident in the retro-gradation of the Playa de  
470 Maspalomas coastline with retreat of up to ~105 m between 1961 and 2006 in response to  
471 SW storm events [Bouzas et al., 2013]. These trends have accounted for a loss of 17% of total  
472 area during this time period (Table 1). Although there is a stable input of sediment into the  
473 system, the coupled natural and anthropogenic dynamics of the environment has led to the  
474 overall decrease in dunefield area, increase in vegetation and deflationary areas, decreased

475 bare sand surfaces, increased distance between dune deposits and the source area, and overall  
476 lowering of the dune topography.

477         The increase in vegetation and subsequent stabilization of the shadow zone can be  
478 attributed to two major factors that have disrupted the natural system. The sediment corridor  
479 has been shifted to flow around the south of the terrace and bypassing the urban shadow  
480 zone. This, coupled with a decrease in competent airflow and sediment flux potential, has led  
481 to widespread colonization of plant species [Hernández-Cordero et al., 2015a,b]. Previous  
482 studies have found that dune vegetation causes an exponential decrease in sediment flux  
483 [Wiggs *et al.*, 1996b; Lancaster and Baas, 1998; Lancaster, 2000]. Lancaster and Baas [1998]  
484 stated that the sediment flux is reduced by 90% of the bare sand surface values when  
485 vegetation covers just 12% of the surface area. Wiggs et al. [1996b] proposed a threshold  
486 vegetation cover of 14% at the dune scale, where the onset of stabilization occurs. Much of  
487 the remaining dunes have become vegetated within the shadow zone. These are interspersed  
488 with intermittent areas of bare sand and deflation surfaces (Fig. 4). Between 1961 and 2006,  
489 vegetation within the shadow zone increased from 6% to 23% of the total area suggesting the  
490 development of a new system equilibrium, identified by large scale stabilization in response  
491 to urbanization.

492         Deflation areas have also increased through time, particularly within the acceleration  
493 zone (Fig. 4). The most significant increase is at the E edge of the dunefield [Hernández-  
494 Calvento et al., 2014]. Hernández et al. [2007] found the accumulation ridge (i.e. coalescence  
495 of incipient barchans into larger barchanoid ridges) has occurred at an increasing distance  
496 from the sediment source area at Playa del Inglés. This has led to a significant rise in  
497 deflation surfaces in this region as small incipient barchan dunes migrate rapidly across the  
498 underlying alluvium layer at up to 35 m yr<sup>-1</sup> [Jackson et al., 2013b]. This in part, can be  
499 attributed to other anthropogenic pressures caused by trampling of the near shore vegetation

500 leading to fragmentation of the foredune and rapid sediment migration further inland  
501 [Hernández-Cordero et al., 2012; Hernández-Calvento et al., 2014]. Near the terminus  
502 section, adjacent to Playa de Maspalomas, an increase in deflationary surfaces has also been  
503 observed on the border between the urban shadow and acceleration zones. These areas  
504 receive reduced sediment inputs due to the deflection of the sediment and airflow across the  
505 dunefield. The rise in deflation areas throughout the dunefield has shifted the system into an  
506 availability-limited state [Kocurek and Lancaster, 1999], and suggests that changes in the  
507 wind energy have resulted in accelerated erosion as dune migration rates exceed sediment  
508 input into the system.

509         Topographic changes, between 2006 and 2011 (Fig. 5), gives an insight into any  
510 sediment deficit occurring at the Maspalomas dunefield. During this time, average climatic  
511 conditions showed slightly elevated  $M$  values in 2009 due to below-average  $P$  and above  
512 average  $PE$  and  $W$  (Fig. 6). Despite this spike in predicted dune activity for 2009, the  
513 lowering of the dune topography and the rates of volumetric changes occurring in the system  
514 remain relatively constant with an average of  $\sim 110,000$  m<sup>3</sup> of net erosion of sediment leaving  
515 the system per year at the sub-decadal scale. Limited sample size only provides a brief  
516 understanding of the sediment budget of the Maspalomas dunefield; however, it indicates its  
517 sediment-limited nature. Given the current available sediment volume of  $14.1 \times 10^6$  m<sup>3</sup> and  
518 the rates of sediment loss, the remaining sediment could be removed within  $\sim 128$  years. Most  
519 of the erosion is concentrated in the acceleration zone, where bare sand surfaces predominate  
520 and are positioned away from the stabilizing effect of vegetation. Here, elevated sediment  
521 flux potential is predicted due to the magnification of regional airflow in response to the  
522 urban geometry. In contrast to the positive feedback identified in the vegetated urban shadow  
523 zone, the impact of urbanization appears to have a negative feedback upon the active dune

524 surfaces leading to both the acceleration of deflation and erosion across much of the dune  
525 surfaces due to modified regional flow dynamics.

## 526 **5.2. Regional Airflow and Sediment Transport Dynamics**

527 Sediment transport prior to urbanization showed increased flux magnitude over the  
528 elevated dune ridges reaching a maximum at the dune crests (Fig. 7a). This is consistent with  
529 streamline compression and acceleration of airflow up the stoss slopes of the dunes, leading  
530 to increased streamwise shear stress at the surface [Frank and Kocurek, 1996a; Wiggs et al.,  
531 1996a; Walker and Nickling, 2002]. Perturbations associated with the first phase of  
532 urbanization (Case 2) caused increased sediment flux magnitude across the acceleration zone  
533 and decreased flux in the urban shadow zone in the NW sector of the dunefield (Fig. 7b).  
534 Subsequent perturbations, during Cases 3 and 4, show similar spatial patterns (Fig. 7c,d),  
535 however, the magnitude increases through time. Following urbanization, flux potential  
536 increased by  $> 0.80$  across the dune crests on the southern tip of the terrace and decreased by  
537 a similar amount in the immediate lee of the buildings. These modified flux patterns has had  
538 a significant impact on the dune dynamics and in- stability identified in the geomorphic  
539 analysis at each time step.

540 The shadow zone has experienced large scale stability due to the reduction of velocity  
541 in the lee of the urban terrace. Recovery of airflow, where surface shear stress normalizes to  
542 upwind values, has been estimated to between  $18-30h$  (where  $h$  is the obstacle height)  
543 [Walker and Nickling, 2003]. Separated flow conditions, downwind of the buildings on the  
544 western edge of the terrace, however, do not recover to upwind flow conditions due to the  
545 limited lateral extent of the dunefield. Thus, modified flux dynamics downwind of the  
546 dunefield never fully re-develop to unperturbed shear stress values allowing for the  
547 widespread stabilization of the urban shadow zone. In contrast, the acceleration zone

548 experiences magnified flux potentials as airflow is compressed and accelerated around the  
549 building geometries. This leads directly to intensified surface shear stress over the majority of  
550 the dune surfaces and explains the accelerated erosion observed at the site through time. As  
551 the dune surfaces are lowered, the recovery of flow occurs at shorter lengths across isolated  
552 interdune locations in the eastern section of the dunefield. This has led to the accelerated  
553 dune migration, increase in deflation areas, and an increase in distance from the source area  
554 to the main accumulation ridge in the central section of the dunefield [Hernández et al., 2007;  
555 Jackson et al., 2013b]. In the central and southwestern sections, sediment flux is also  
556 intensified and these locations have displayed the highest rates of net topographic lowering  
557 (Fig. 5a,b).

558         Significant  $\delta\theta$  has also been observed at Maspalomas where largely homogeneous  
559 flow directions are observed during the pre-urbanization phase to highly deflected flow in  
560 subsequent urbanization phases. The initial perturbations caused by the first phase of  
561 urbanization, deflected flow northerly upwind of the terrace moving sediment towards the S  
562 before flow moving around the terrace redirects easterly moving sediment towards the W in  
563 downwind locations (Fig. 8b). Following each phase of urbanization and resulting flow  
564 perturbations (i.e. Cases 3 and 4) we see, relative to pre-urbanized flow directions, a  
565 magnification of flow deflection of up to  $25^\circ$  upwind of the terrace,  $21^\circ$  downwind of the  
566 terrace, and  $172^\circ$  in the urban induced recirculation cell relative to pre-urbanized flow  
567 directions. These results correspond well with those presented by Hernández-Calvento et al.  
568 [2014] who found a  $15^\circ - 20^\circ$  deflection of flow upwind of the terrace before flow shifted  
569 towards the S in downwind locations. The geomorphic significance of these perturbations is  
570 the modification of primary (i.e. stoss side flow) and secondary (i.e. lee side flow) at the dune  
571 length scale and the overall truncation of the sediment pathway through the system at the  
572 dunefield scale.



573 As wind moves across the individual dune topography, the incident angle of airflow  
574 has significant impact on the secondary airflow dynamics that occur in the lee. Sweet and  
575 Kocurek [1990] found that incident angles of  $90^\circ \pm 15^\circ$  produced the development of  $15^\circ -$   
576  $75^\circ$  roller vortices, and deflected flow by  $10^\circ - 70^\circ$ . These in turn have significant impact on  
577 sediment transport dynamics with recirculating turbulent vortices recycling sediment back  
578 towards the lee slope and maintaining characteristic dune-form geometries [Tsoar and  
579 Yaalon, 1983; Tsoar et al., 1985; Sweet and Kocurek, 1990; Frank and Kocurek, 1996b;  
580 Walker, 2000; Smith et al., 2017]. For example, the deflection of lee-side flow direction  
581 increases through time due to the upwind flow being forced to a more northerly angle with  
582  $\delta\theta$  of up to  $25^\circ$  during Case 4 (Fig. 8d), modifying the approach angle on the stoss and thus  
583 potentially modifying the secondary airflow dynamics (e.g. deflected flow vs. recirculating  
584 vortices) [Lynch et al., 2010]. At the dunefield scale, surface flow direction and subsequent  
585 sediment inputs into the system from Playa del Inglés are therefore being forced towards the  
586 south accumulating mainly in the central section of the dunefield. Here, velocity acceleration  
587 and deflection towards the S leads to a shortened sediment corridor in which the migration of  
588 dunes can take place. This potentially leads to the reduction of residence time of sediment  
589 being fed into the dunefield, further amplifying the sediment deficit recorded at Maspalomas.

590 Following urbanization there has been an increase of  $\delta TI$ , primarily on the lee slopes  
591 of elevated dune crests in the central section of the dunefield and in the interdune areas where  
592 secondary airflow patterns are observed. This increase in  $\delta TI$  can lead to intermittent  
593 sediment transport due to the momentum transfer of the overlying turbulent wake zone to the  
594 surface near the point of reattachment [Walker and Nickling, 2002; Baddock et al., 2007].  
595 Our results also show elevated values of  $\delta TI$  on the lee slopes providing elevated erosive  
596 potential due to destabilizing concave curvature in mobilizing sediment under low threshold  
597 values [Wiggs et al., 1996a; Smith et al., 2017]. Coherent flow structures are also apparent

598 and are identified by an elevated  $\delta TI$  signature (Fig. 9a,b,c,d). Smith et al. [2017] found  
599 evidence of coherent counter-rotating vortices that develop over barchan dunes in highly  
600 turbulent secondary airflow conditions in the lee. These counter-rotating vortices have also  
601 been modelled in terrestrial [Feng and Ning, 2010] and subaqueous [Omidyeganeh et al.,  
602 2013] dunes. The prevalence of these structures in the lee of dune crests (Fig. 10a) displays a  
603 commonality in turbulent flow that likely has a deterministic impact on dune morphology and  
604 dynamics. Smith et al. [2017] suggested that these flow structures could work to maintain the  
605 characteristic crescentic shape of barchan dunes by redirecting sediment back to the base of  
606 the lee slope centreline and laterally away towards the inner barchan arms across the lee  
607 slope.

608         Across the urban area and the downwind urban shadow zone, highly turbulent airflow  
609 conditions develop (Figs. 9b,c,d; 10b). Increased surface roughness due to urbanization  
610 caused an increase in  $\delta TI$  compared to the relatively stable flow conditions observed during  
611 pre-urbanization (Fig. 9a). Well-developed recirculation cells form in the immediate lee of  
612 the terrace with a range of structures including roller and counter-rotating vortices (Fig. 10a).  
613 Increased  $TI$  can lead to the redistribution of pre-existing sediment deposits in the urban  
614 shadow zone evidenced by low magnitude erosion and deposition between 2006 and 2011  
615 (Fig. 5a,b), despite increased vegetation and the reduced surface velocity. Although increased  
616 turbulence may rework existing sediment, fully turbulent flow conditions in the urban  
617 shadow zone coupled with limited recovery distance and lack of dune deposits extending into  
618 the boundary layer impedes significant sediment transport in this region as flow has  
619 insufficient length to recover [Walker and Nickling, 2002].

## 620 **6. Conclusion**

621 This study provides evidence of regional airflow perturbations and geomorphic  
622 implications of anthropogenic structures on IBL flow and dune dynamics. The main  
623 conclusions are:

- 624 1. Episodic variability in climatic conditions cannot account for the observed changes in  
625 the Maspalomas dunefield. Simultaneous stabilization seen from increases in  
626 vegetation and accelerated activity seen by sediment deficit is due to the  
627 anthropogenic pressure caused by the intrusion of the urban geometry into the IBL.
- 628 2. Human-modified regional airflow and sediment transport patterns have led directly to  
629 a dichotomy in dunefield evolution (i.e. both increased stabilization and acceleration  
630 of erosion) at the decadal scale. This can be attributed to the increasingly magnified  
631 perturbations of regional airflow by urbanization during different phases of  
632 construction causing two distinct geomorphic zones (i.e. the urban shadow zone and  
633 acceleration zone).
- 634 3. The urban shadow zone, located downwind of the urban terrace, is largely a stabilized  
635 dune system with  $q'$  progressively declining due to the reduction in near surface  
636 velocity. The sediment input pathway from the source area to the NW sector has  
637 largely been cut off with  $\delta\theta$  redirecting sediment towards the central section of the  
638 dunefield. Also, construction of an impenetrable urban surface further starves this  
639 area of sediment, allowing for further colonization of plant species due to the  
640 reduction dune migration rates.
- 641 4. The acceleration zone, where the active dunes are migrating, has experienced large  
642 scale modifications in  $\delta\theta$ , forcing sediment towards the south and  $\delta q'$  thus increasing  
643 the erosive potential across much of the active surface. This has led to a progressive  
644 deficit in sediment by accelerating erosion and shortening the sediment pathway

645 through the system, effectively reducing the residence time sediment moves from the  
646 source to the terminus.

647 5.  $\delta TI$  was intensified following urbanization, primarily on the lee slopes and interdune  
648 areas. This helps promote intermittent erosion and increased dune spacing, leading to  
649 the potential for further acceleration of dune migration and erosion within the system.  
650 Coherent turbulent flow structures were identified in the lee of elevated dune crests  
651 and downwind of the urban terrace where the development of counter-rotating  
652 vortices formed. The ubiquity of these features suggests that they have an important  
653 role in both characteristic individual barchan dune form and indeed larger dunefield  
654 dynamics.

## 655 **Acknowledgements**

656 The authors would like to thank the GFyMA Group (IOCAG-ULPGC) for providing  
657 resources and logistical support. Expert guidance on CFD modelling and OpenFOAM were  
658 provided by Meiring Beyers (Klimaat Consulting & Innovation Inc.). Research funding were  
659 provided by the University of Ulster Vice Chancellor's Research Scholarship (VCRS). This  
660 work is a contribution towards project CSO2013-43256-R funded by the R&D+I (innovation)  
661 Spanish National Programme and a contribution to the UK Natural Environment Research  
662 Council grant NE/F019483/1. Any additional information can be requested from the  
663 corresponding author at smith-a22@email.ulster.ac.uk.

## 664 **References**

665 Alcántara-Carrió, J., Fontán, A. 2009. Factors Controlling the Morphodynamics and  
666 Geomorphologic Evolution of a Cuspate Foreland in a Volcanic Intraplate Islands  
667 (Maspalomas, Canary Islands). *Journal of Coastal Research* 56: 683-687.

668 Alonso I., Hernández Calvento L., Alcántara-Carrió J., Cabrera-Vega L.L., Yanes A. 2011.  
669 Los grandes campos de dunas actuales de Canarias. In: Sanjaume, E. y Gracia, F.J  
670 (Eds.): *Las dunas en España*. Madrid: Sociedad Española de Geomorfología: 467-  
671 495.

672 Baddock, M.C., Livingstone, I., Wiggs, G.F.S. 2007. The geomorphological significance of  
673 airflow patterns in transverse dune interdunes. *Geomorphology* (87): 322-336.

674 Bagnold, R.A. 1941. The physics of wind-blown sand and desert dunes. Methuen, London,  
675 265 (10).

676 Bagnold, R.A. 1973. The nature of saltation and of 'bed-load' transport in water. In  
677 Proceedings of the Royal Society of London A: Mathematical, Physical and  
678 Engineering Sciences. Vol. 332. no. 1591: 473-504.

679 Bai, J.J., Park, S.B. 2009. Urban Flow and Dispersion Simulation Using a CFD Model  
680 Coupled to a Mesoscale Model. *Journal of Applied Meteorology and Climatology* (8):  
681 1667-1681.

682 Bauer, B.O., Walker, I.J., Baas, A.C.W., Jackson, Derek, McKenna-Neuman, C., Wiggs,  
683 G.F.S. and Hesp, P.A. (2013) Critical Reflections on the Coherent Flow Structures  
684 Paradigm in Aeolian Geomorphology. In: Venditti, J.G., Best, J.L., Church, M.,  
685 Hardy, R.J. (Eds.), *Coherent Flow Structures at Earth's Surface*, Wiley, pp. 111-134.  
686 ISBN: 978-1-119-96277-9.

687 Blocken, B., Janssen, W.D., van Hoof, T. 2012. CFD simulation for pedestrian wind comfort  
688 and wind safety in urban areas: General decision framework and case study for the  
689 Eindhoven University campus. *Environmental Modelling & Software* (30): 15-34.

690 Bouzas, A.F., Alcántara-Carrió, J., Montes, I.M., Ojeda, A.B., Albarracín, S., de Rada,  
691 J.R.D., Salgado, J.R. 2013. Distribution and thickness of sedimentary facies in the  
692 coastal dune, beach, and nearshore sedimentary system at Maspalomas, Canary  
693 Islands. *Geo-Marine Letters* (33;2-3): 117-127.

694 Bullard, J.E., Thomas, D.S.G., Livingstone, I., Wiggs, G.F.S. 1997. Dunefield activity and  
695 interactions with climatic variability in the southwest Kalahari Desert. *Earth Surface  
696 Processes and Landforms* (22): 164-174.

697 Cabrera-Vega, L.L., Cruz-Aver, N., Hernández-Calvento, L., Hernández-Cordero, A.I.,  
698 Fernández-Cabrera, E. 2013. Morphological changes in dunes as an indicator of  
699 anthropogenic interferences in arid dune fields. *Journal of Coastal Research*. (65):  
700 1271-1276.

701 Fadl, M.S., Karadelis, J. 2013 CFD Simulations for Wind Comfort and Safety in Urban Area:  
702 A Case Study of Coventry University Central Campus. *International Journal of  
703 Architecture, Engineering, and Construction* (2): 131-143.

704 Feng, S., Ning, H. 2010. Computational simulations of blown sand fluxes over the surfaces of  
705 complex microtopology. *Environmental Modelling & Software* (25): 362-367.

706 Fontán, A., Alcántara-Carrió, J., Correa, I.D. 2012. Combined beach-inner shelf erosion in  
707 short and medium term (Maspalomas, Canary Islands). *Geologica Acta* (10; 4): 411-  
708 426.

709 Frank, A. and Kocurek, G. 1996 (a). Airflow up the stoss slope of sand dunes: limitations of  
710 current understanding. *Geomorphology* (17): 47–54.

711 Frank, A., Kocurek, G. 1996 (b). Toward a model for airflow on the lee side of Aeolian  
712 dunes. *Sedimentology* (43): 451-458.

713 Gundlach, E.R., Siah, S.J. 1987. Cause and Elimination of the Deflation Zones Along the  
714 Atlantic City (New Jersey) Shoreline. *Coastal Zone'87*: 1357-69.

715 Hanna, S.R., Brown, M.J., Camelli, F.E., Chan, S.T., Coirier, W.J., Hansen, O.R., Huber,  
716 A.H., Kim, S., Reynolds, R.M. 2006. Detailed Simulations of Atmospheric Flow and  
717 Dispersion in Downtown Manhattan An Application of Five Computational Fluid  
718 Dynamics Models. *Bulletin of the American Meteorological Society* (December  
719 2006): 1713-1726.

720 Hernández Calvento, L. 2006. Diagnóstico sobre la Evolución del Sistema de Dunas de  
721 Maspalomas (1960-2000). Ed. Cabildo de Gran Canaria, Las Palmas de Gran Canaria.

722 Hernández, L., Alonso, I., Sánchez-Pérez, I., Alcántara-Carrió, J., Montesdeoca, I. 2007.  
723 Shortage of sediments in the Maspalomas dune field (Gran Canaria, Canary Islands)  
724 deduced from the analysis of aerial photographs, foraminiferal content, and sediment  
725 transport trends. *Journal of Coastal Research* (23; 4): 993-999.

726 Hernández-Calvento, L., Jackson, D.W.T., Medina, R., Hernández-Cordero, A.I., Cruz, N.,  
727 Requejo, S. 2014. Downwind effects on an arid dunefield from an evolving urbanised  
728 area. *Aeolian Research* (15): 301-309.

729 Hernández-Cordero, A.I., Pérez-Chacón, E., Hernández-Calvento, L., 2012. La investigación  
730 como soporte de la gestión: el ejemplo de la duna costera (foredune) de Maspalomas  
731 (Gran Canaria, Islas Canarias). In: Rodríguez-Perea, A., Pons, G.X., ROig-Munar,  
732 F.X., Martín-Prieto, J.A., Mir-Gual, M., Cabrera, J.A. (Eds.). *La gestión integrada de  
733 playas y dunas: experiencias en Latinoamérica y Europa. Monografies de la Societat  
734 d'Història Natural de les Balears 19. Societat d'Història Natural de las Balears, PM,  
735 Spain: 289-306.*

736 Hernández-Cordero, A.I., Pérez-Chacón, E., Hernández-Calvento, L. 2015. Vegetation  
737 disturbance on the coast, and aeolian geomorphic processes and landforms in a  
738 transgressive arid coastal dune system. *Physical Geography* (30; 1): 60-83.

739 Hernández-Cordero, A.I., Hernández-Calvento, L., Espino, E.P.C. 2015 (b). Relationship  
740 between vegetation and dune mobility in an arid transgressive coastal system,  
741 Maspalomas, Canary Islands. *Geomorphology* (238): 160-176.

742 Hugenholtz, C.H., Wolfe, S.A. 2005. Recent stabilization of active sand dunes on the  
743 Canadian prairies and relation to recent climate variations. *Geomorphology* (68; 1-2):  
744 131-147.

745 Jackson, P.S., Hunt, J.C.R. 1975. Turbulent wind flow over a low hill. *Quarterly Journal of*  
746 *the Royal Meteorological Society* 101(430): 929-955.

747 Jackson, D.W.T., Beyers, M., Delgado-Fernandez, I., Baas, A.C.W., Cooper, J.A.G. and  
748 Lynch, K. 2013a. Airflow reversal and alternating corkscrew vortices in foredune  
749 wake zones during perpendicular and oblique offshore winds. *Geomorphology* (187):  
750 86-93.

751 Jackson, D.W.T., Cruz-Avero, N., Smyth, T., Hernández-Calvento, L. 2013b. 3D airflow  
752 modelling and dune migration patterns in an arid coastal dune field. *Journal of Coastal*  
753 *Research, Special Issue* (65): 1301-1306.

754 Jackson, N.L., Nordstrom, K.F. 2011. Aeolian sediment transport and landforms in managed  
755 coastal systems: A review. *Aeolian Research* (38): 2011.

756 Kim, J.J., Fernando, H.J.S. 2003. A CFD Model for Simulating Urban Flow and Dispersion.  
757 *Journal of Applied Meteorology* (42): 1636-1648.



- 758 Kocurek, G., Lancaster, N. 1999. Aeolian system sediment state: theory and Mojave Desert  
759 Kelso dune field example. *Sedimentology* (46): 505-515.
- 760 Lancaster, N. 1988. Development of linear dunes in southwestern Kalahari, Southern Africa.  
761 *Journal of Arid Environments* (14): 233-244.
- 762 Lancaster, N. 1997. Response of eolian geomorphic systems to minor climate change:  
763 examples from the southern Californian deserts. *Geomorphology* (19): 333-347.
- 764 Lancaster, N., Baas, A. 1998. Influence of vegetation cover on sand transport by wind: Field  
765 studies at Owens Lake, California. *Earth Surface Processes and Landforms* (23): 69-  
766 82.
- 767 Lancaster, N., Helm, P. 2000. A Test of Climatic index on dune mobility using measurements  
768 from the southwestern United States. *Earth Surface Processes and Landforms* (25):  
769 197-207.
- 770 Lynch, K., Jackson, D.W., Cooper, J.A.G. 2010. Coastal foredune topography as a control on  
771 secondary airflow regimes under offshore winds. *Earth Surface Processes and*  
772 *Landforms* (35.3): 344-353.
- 773 Lynch, K., Delgado-Fernandez, I., Jackson, Derek, Cooper, Andrew, Baas, A.C.W and  
774 Beyers, J.H.M. 2013. Alongshore variation of aeolian sediment transport on a beach  
775 under offshore winds. *Aeolian Research* (8): 11-18.
- 776 Lynch, K., Jackson, D.W.T. and Cooper, J.A.G. 2016. The fetch effect on aeolian sediment  
777 transport on a sandy beach: a case study from Magilligan strand, Northern Ireland.  
778 *Earth Surface Processes and Landforms* (41): 1129-1135.

- 779 Meir, A., Tsoar, H. 1996. International Borders and Range Ecology: The Case of Bedouin  
780 Transborder Grazing. *Human Ecology* (24): 39-64.
- 781 MMA, 2007. *Estudio integral de la playa y dunas de Maspalomas (Gran Canaria)*. Technical  
782 report. Ministerio de Medio Ambiente, Gobierno de España.
- 783 Murakami, S., Ooka, R., Mochida, A., Yoshida, S., Kim, S. 1999. CFD analysis of wind  
784 climate from human scale to urban scale. *Journal of Wind Engineering and Industrial*  
785 *Aerodynamics* (81): 57-81.
- 786 Muhs, D.R., Maat, P.B. 1993. The potential response of eolian sands to greenhouse warming  
787 and precipitation reduction on the Great Plains of the U.S.A. *Journal of Arid*  
788 *Environments* (25): 351-361.
- 789 Muhs, D.R., Reynolds, R.L., Been, J., Skipp, G. 2003. Eolian sand transport pathways in the  
790 southwestern United States: importance of the Colorado River and local sources.  
791 *Quaternary International* (104): 3-18.
- 792 Nordstrom, K.F., McCluskey, J.M. 1984. Considerations for control of house construction in  
793 coastal dunes. *Coastal Management* (12): 385-402.
- 794 Nordstrom, K.F. 1994. Beaches and dunes of human-altered coasts. *Progress in Physical*  
795 *Geography* (18): 497-516.
- 796 Nordstrom, K.F., Jackson, N.L. 1998. Aeolian transport of sediment on a beach during and  
797 after rainfall, Wildwood, NJ, USA. *Geomorphology* (22): 151-157.
- 798 Omidyeganeh, M., Piomelli, U., Christensen, K.T., Best, J.L. 2013. Large Eddy Simulation of  
799 flow over barchans dunes. *Marine and River Dune Dynamics* (15 & 16): 191-198.

800 Owen, P. R. 1964. Saltation of uniform grains in air. *Journal of Fluid Mechanics* 20(2): 225-  
801 242.

802 Pullen, J., Boris, J.P., Young, T., Patnaik, G., Iselin, J. 2005. A comparison of contaminant  
803 plume statistics from a Gaussian puff and urban CFD model for two large cities.  
804 *Atmospheric Environment* (39): 1049-1068.

805 Quevedo Medina, U., Hernández Calvento, L. 2014. Evolución reciente de la línea de costa  
806 de un sistema playa-dunas deficitario. Maspalomas, Gran Canaria. In: Ramón Morte,  
807 A. et cols. (Eds.): *Tecnologías de la información geográfica para nuevas formas de*  
808 *ver el territorio*. Alicante: Universidad de Alicante, España: 163-171.

809 Richards, P. J., Hoxey, R.P. 1993. Appropriate boundary conditions for computational wind  
810 engineering models using the k- $\epsilon$  turbulence model. *Journal of Wind Engineering and*  
811 *Industrial Aerodynamics* (46 & 47): 145-153.

812 Richards, P. J., Hoxey, R. P. 2012. Pressures on a cubic building – Part 1: Full-scale results.  
813 *Journal of Wind Engineering and Industrial Aerodynamics* (102): 72-86.

814 Sabatino, S.D., Buccolieri, R., Pulvirenti, B., and Britter, R. 2007. Simulations of pollutant  
815 dispersion within idealised urban-type geometries with CFD and integral models.  
816 *Atmospheric Environment* (41): 8316-8329.

817 Sauermann, G., Kroy, K., Herrmann, H.J. 2001. Continuum saltation model for sand dunes.  
818 *Physical Review E* 64(3): 031305.

819 Sauermann, G., Andrade Jr., J.S., Maia, L.P., Costa, U.M.S., Araújo, A.D., Herrmann, H.J.  
820 2003. Wind velocity and sand transport on a barchan dune. *Geomorphology* (54):  
821 245-255.

- 822 Smith, A.B., Jackson, D.W.T, Cooper, J.A.G. 2017. Three-dimensional airflow and sediment  
823 transport patterns over barchan dunes. *Geomorphology* (278): 28-42.
- 824 Smyth, T.A.G. 2016. A review of Computational Fluid Dynamics (CFD) airflow modelling  
825 over aeolian landforms. *Aeolian Research* (22): 153-164.
- 826 Stetler, L.D., Gaylord, D.R. 1996. Evaluating eolian-climatic interactions using a regional  
827 climate model from Hanford, Washington (USA). *Geomorphology* (17): 99-113.
- 828 Sweet, M.L., Kocurek, G. 1990. An empirical model of aeolian dune lee-face airflow.  
829 *Sedimentology* (37): 1023-1038.
- 830 Thomas, D.S.G., Knight, M., Wiggs, G.F.S. 2005. Remobilization of southern African desert  
831 dune systems by twenty-first century global warming. *Nature Letters* (435): 1218-  
832 1221.
- 833 Thornthwaite, C.W. 1948. An Approach toward a Rational Classification of Climate.  
834 *Geographical Review* (38): 55-94.
- 835 Troen, I, Petersen, E.L. 1989. European wind atlas. Roskilde: Riso National Laboratory  
836 (1989): 1.
- 837 Tsoar, H., Yaalon, D.H. 1983. Deflection of sand movement on a sinuous longitudinal (seif)  
838 dune: use of fluorescent dye as tracer. *Sedimentary Geology* (36): 25-39.
- 839 Tsoar, H., Rasmussen, K.R., Sorensen, M., Willets, B.B. 1985. Laboratory studies of flow  
840 over dunes. Proceedings of international workshop on the physics of blown sand.  
841 Department of Theoretical Statistics, Institute of Mathematics, University of Aarhus.  
842 327-50.

843 Tsoar, H., Levin, N., Porat, N., Maia, L.P., Herrmann, H.J., Tatumi, S.H., Claudino-Sales, V.  
844 2009. The effect of climate change on the mobility and stability of coastal and sand  
845 dunes in Ceará State (NE Brazil). *Quaternary Research* (71): 217-226.

846 UNCCD. United Nations Convention to Combat Desertification, Intergovernmental  
847 Negotiating Committee For a Convention to Combat Desertification, Elaboration of  
848 an International Convention to Combat Desertification in Countries Experiencing  
849 Serious Drought and/or Desertification, Particularly in Africa. U.N. Doc.  
850 A/AC.241/27. 33 I.L.M. 1328 New York: United Nations; 1994.

851 Vallejo I., Hernández Calvento L., Ojeda J., Máyer P., Gómez Molina A. 2009.  
852 Caracterización morfométrica y balance sedimentario en el sistema de dunas de  
853 Maspalomas (Gran Canaria) a partir de datos LiDAR. *Revista de la Sociedad  
854 Geológica de España* 22 (1-2): 57-65.

855 Walker, I.J. 2000. Secondary airflow and sediment transport in the lee of transverse dunes,  
856 Ph. D.  
857 Thesis, Department of Geography, University of Guelph. 1-256.

858 Walker, I.J., Nickling, W.G. 2002. Dynamics of secondary airflow and sediment transport  
859 over and in the lee of transverse dunes. *Progress in Physical Geography* (26): 47-75.

860 Walker I.J., Nickling, W.G. 2003. Simulation and measurement of surface shear stress over  
861 isolated and closely spaced transverse dunes in a wind tunnel. *Earth Surface Processes  
862 and Landforms* (28): 1111-1124.

863 White, B.R., Mounla, H. 1991. An experimental study of Froude number effect on wind-  
864 tunnel saltation. *Aeolian Grain Transport* (1): 145-157.

865 Wiggs, G.F.S., Thomas, D.S.G., Bullard, J.E. 1995. Dune mobility and vegetation cover in  
866 the southwest Kalahari Desert. *Earth Surface Processes and Landforms* (20): 515-529.

867 Wiggs, G.F.S, Livingstone, I., Warren, A. 1996 (a). The role of streamline curvature in sand  
868 dune dynamics: evidence from field and wind tunnel measurements. *Geomorphology*  
869 (17): 29-46.

870 Wiggs, G.F.S., Livingstone, I., Thomas, D.S.G., Bullard, J.E. 1996 (b). Airflow and  
871 roughness characteristics over partially vegetated linear dunes in the southwest  
872 Kalahari Desert. *Earth Surface Processes and Landforms* 21(1): 19-34.

873 Wolfe, S.A. 1996. Impact of increased aridity on sand dune activity in the Canadian Prairies.  
874 *Journal of Arid Environments* (36): 421-432.

875 Yizhaq, H., Ashkenazy, Y., Tsoar, H. 2007. Why do active and stabilized dunes coexist under  
876 the same climatic conditions? *Physical Review Letters* (98): 188001-4.

	<b>Dunefield km<sup>2</sup></b>	<b>Bare Sand km<sup>2</sup></b>	<b>Beach km<sup>2</sup></b>	<b>Vegetation km<sup>2</sup></b>	<b>Deflation km<sup>2</sup></b>
<b>1961</b>	4.42	3.93 <b>(90%)</b>	0.26 <b>(6%)</b>	0.10 <b>(2%)</b>	0.11 <b>(2%)</b>
<b>1977</b>	3.70	3.04 <b>(82%)</b>	0.18 <b>(5%)</b>	0.27 <b>(7%)</b>	0.20 <b>(5%)</b>
<b>1987</b>	3.63	2.93 <b>(81%)</b>	0.27 <b>(7%)</b>	0.24 <b>(7%)</b>	0.18 <b>(5%)</b>
<b>2006</b>	3.67	2.59 <b>(70%)</b>	0.40 <b>(11%)</b>	0.41 <b>(11%)</b>	0.27 <b>(7%)</b>

877  
878 Table 1: Change in the areal extent (km<sup>2</sup>) for the dunefield, bare sand, beach, vegetation, and  
879 deflation surfaces during the years 1961, 1977, 1987, and 2006.

880 Figure 1: Maspalomas dunefield is located on the southern coast of Gran Canaria, Canary  
881 Islands, Spain (A,C). The competent wind regime (i.e. >5.5 ms<sup>-1</sup>) was recorded at an AEMET  
882 meteorological weather station located 0.6 km to the west of Playa de Maspalomas. The wind  
883 regime, between 2004-2015, was bi-modal with westerly and easterly wind exceeding  
884 threshold values (B).

885 Figure 2: Maspalomas has experienced widespread urbanization between 1961 (A) and 2006  
886 (C). In 1961 (B), climbing dunes were able to bypass the elevated terrace surface, feeding  
887 downwind areas with sediment. Following urbanization of the terrace surface (D), this  
888 sediment corridor has been disrupted and continual urbanization has further modified the  
889 regional airflow dynamics at the Maspalomas dunefield.

890 Figure 3: DEM of the Maspalomas dunefield (2006) with the three major phases of  
891 construction across the terrace surface including 1977, 1987, and 2006 (A). A castellated  
892 mesh was generated with four levels of progressive cell refinement set towards the coupled  
893 model surface, maintaining a representative surface gradient of the complex dune topography  
894 and urban geometries (B).

895 Figure 4: Land cover change occurring at Maspalomas for the years 1961 (A), 1977 (B), 1987  
896 (C), and 2006 (D). Changes in the areal extent of the dunefield, urban shadow zone (i.e.  
897  $< \delta q'$ ), acceleration zone (i.e.  $> \delta q'$ ), beach, vegetation, and deflation surfaces have  
898 changed through time.

899 Figure 5: Topographic changes, identified from aerial LiDAR surveys, between the years  
900 2006-2008 (A) and 2008-2011(B). The 2011 LiDAR dataset was unfiltered and vegetation  
901 was considered null due to overestimation of the 'bare-earth' surface.

902 Figure 6: The dune mobility index ( $M$ ) for the Maspalomas dunefield between the years 1957  
903 to 2011.  $M$  values largely remain  $>200$  which are classified as fully active dunes with limited  
904 stabilization due to vegetation.

905 Figure 7: Sediment flux potential ( $q'$ ) during Case 1 and sediment flux perturbation  
906 ( $\delta q'$ ) following multiple phases of urbanization for Cases 2-4 (B,C,D).

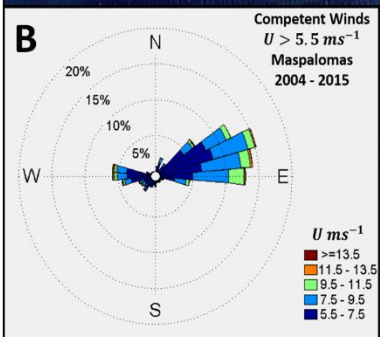
907 Figure 8: Surface airflow direction ( $\theta$ ) during Case 1 (A) and airflow direction perturbations  
908 ( $\Delta\theta$ ) following multiple phases of urbanization for Cases 2-4 (B,C,D). Arrows indicate the  
909 deflection in degrees between the pre-urbanization period (C1) and each subsequent  
910 urbanization period (C2,C3,C4).

911 Figure 9: Surface turbulence intensity ( $TI$ ) during Case 1 (A) and turbulence intensity  
912 perturbations ( $\delta TI$ ) following multiple phases of urbanization for Cases 2-4 (B,C,D).

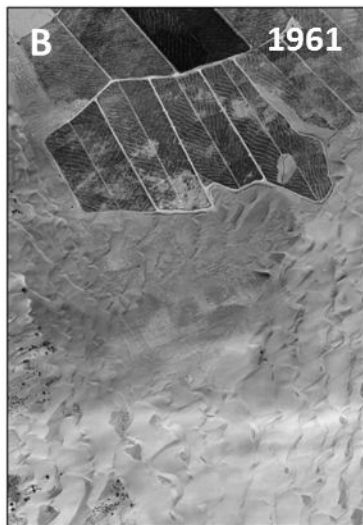
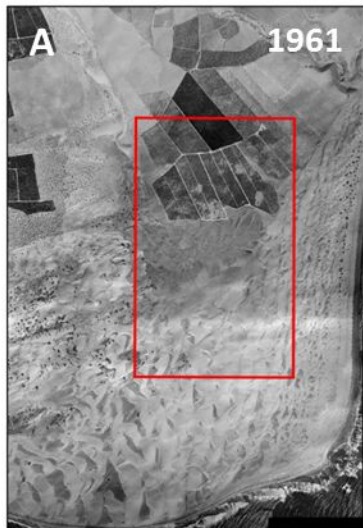
913 Figure 10: Turbulent flow conditions including counter-rotating vortices represented by  
914 surface vectors showing the angle of flow between the streamwise ( $u$ ) and spanwise ( $v$ ) flow  
915 components (A,B).



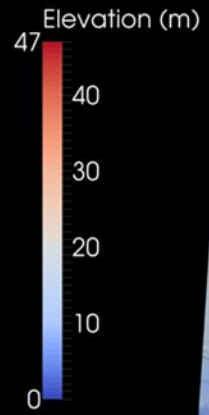
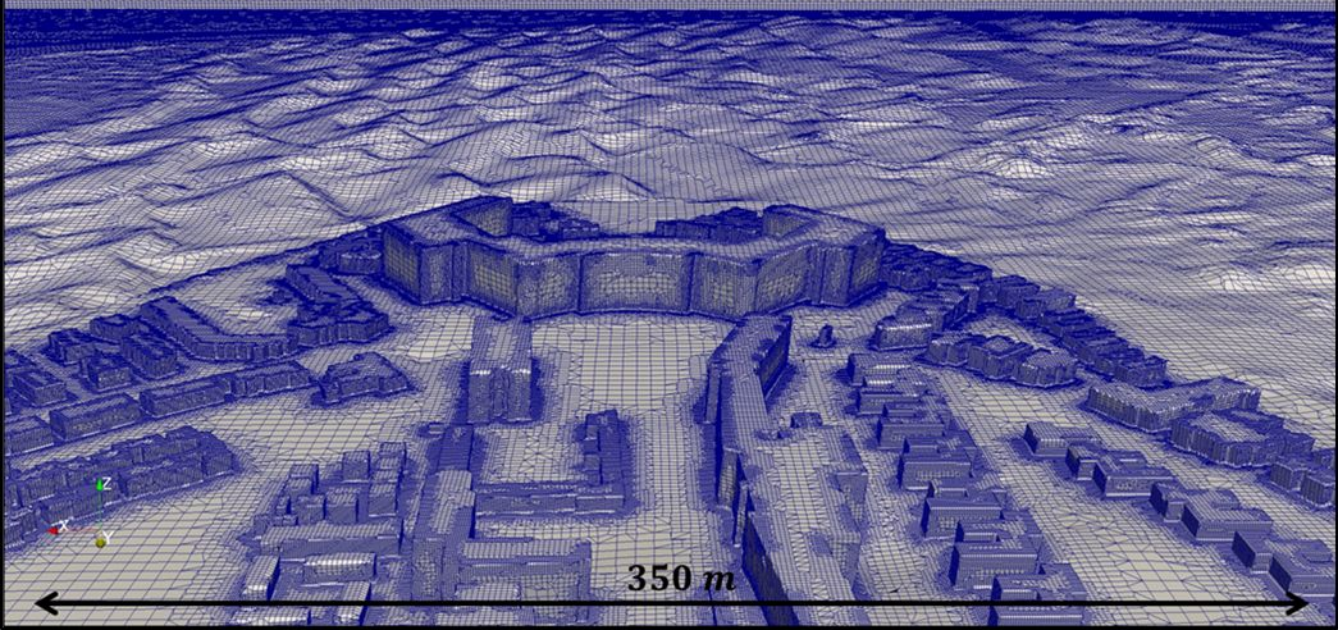
**Figure 1.**



**Figure 2.**



**Figure 3.**

**A****B**

**Figure 4.**

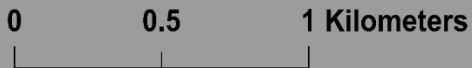
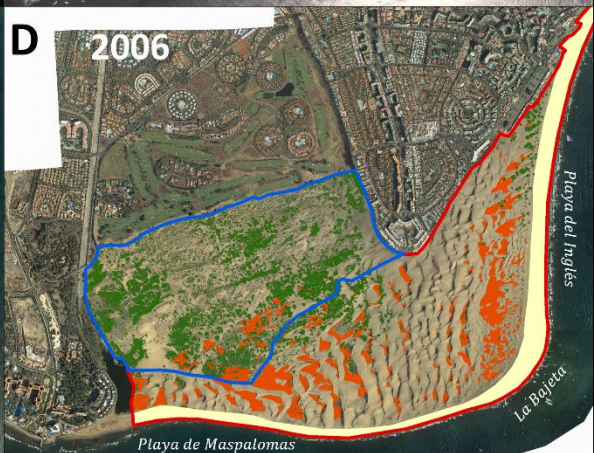
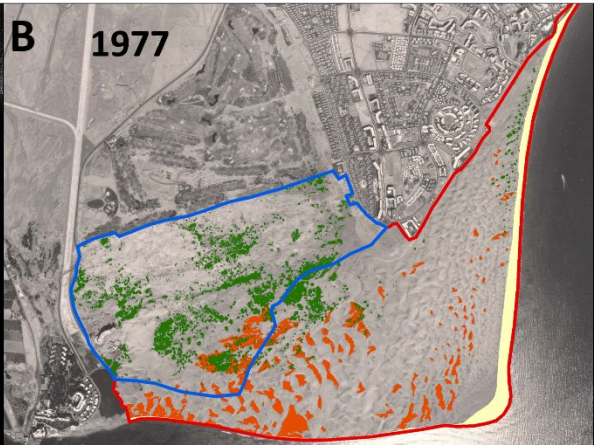
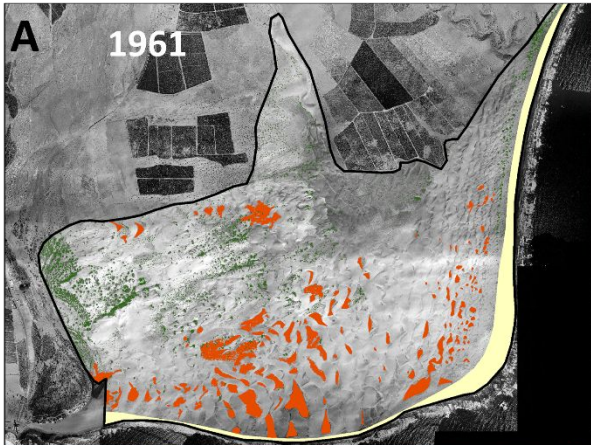
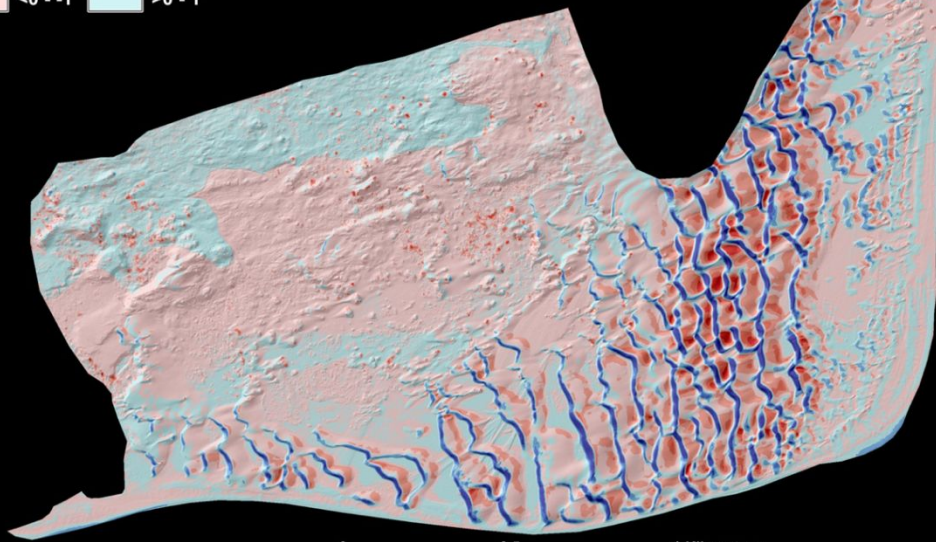




**Figure 5.**

## Topographic Change 2006 - 2008

### Elevation Change (m)



## Topographic Change 2008 - 2011

### Elevation Change (m)



### Vegetation (No Data)

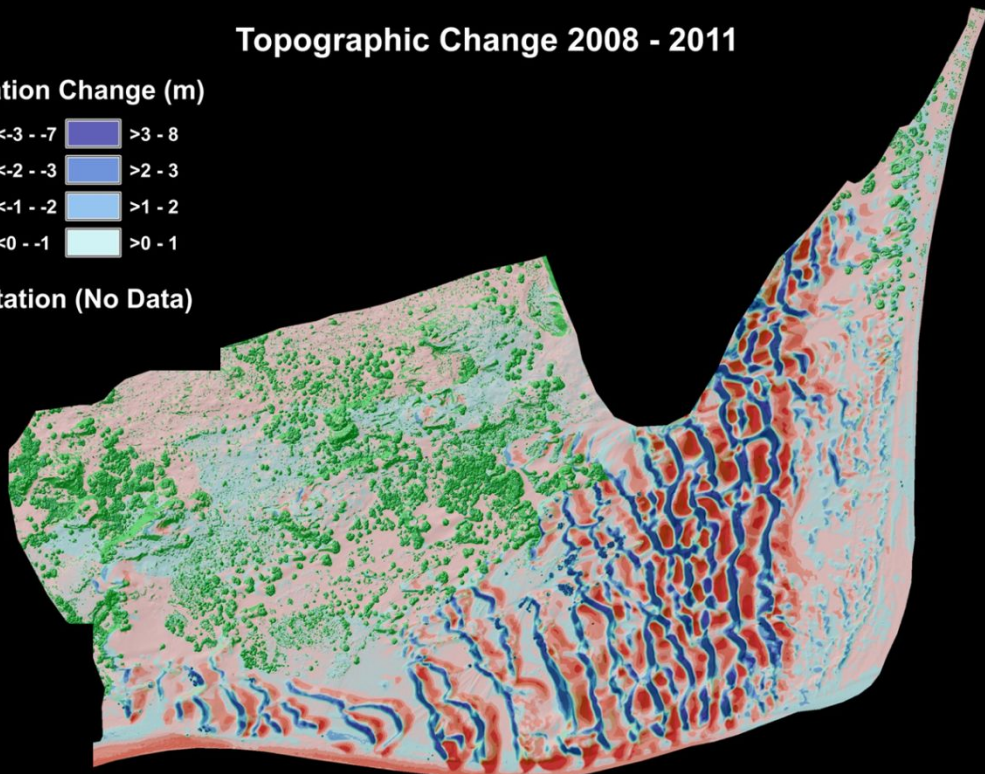


**Figure 6.**

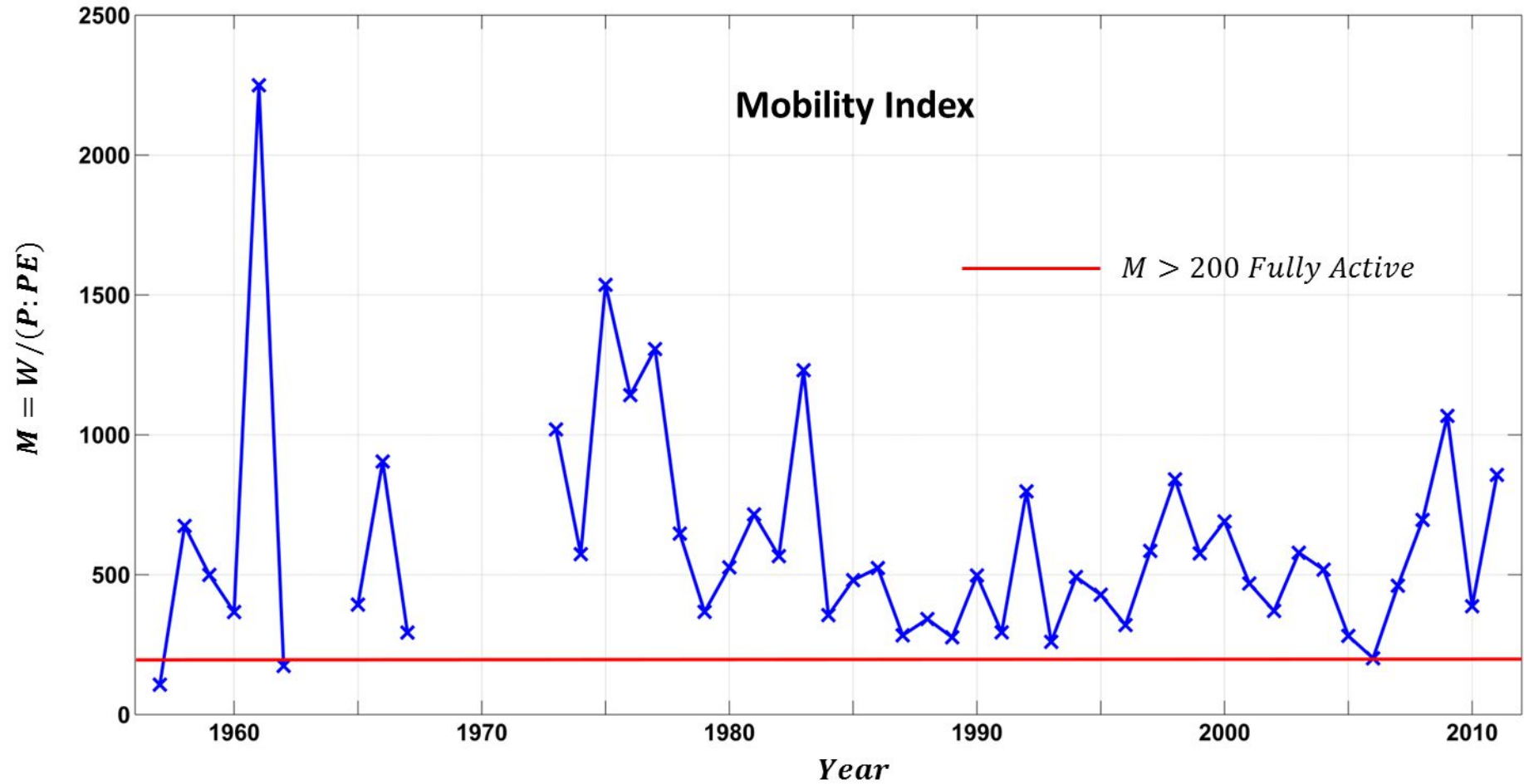
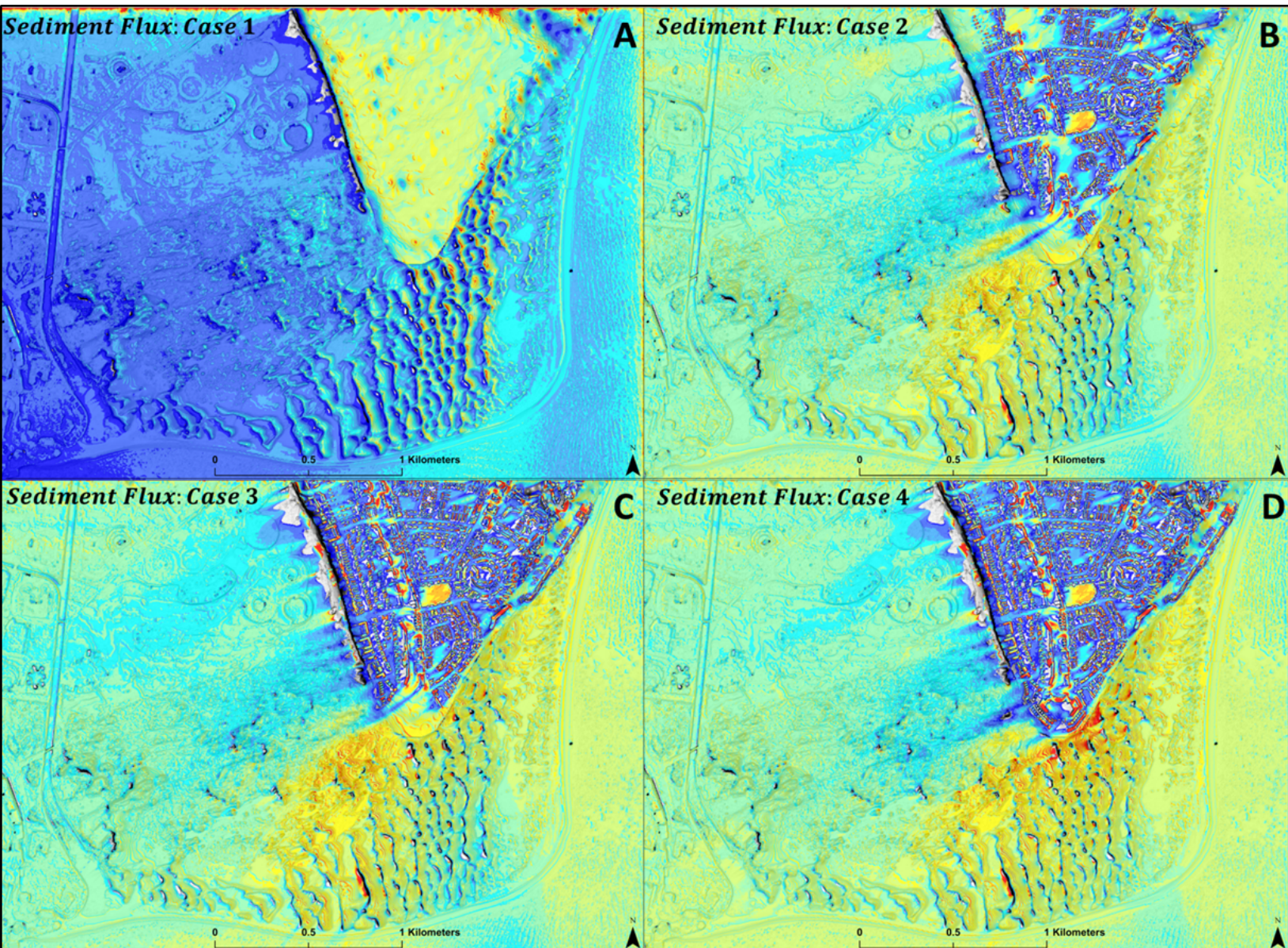
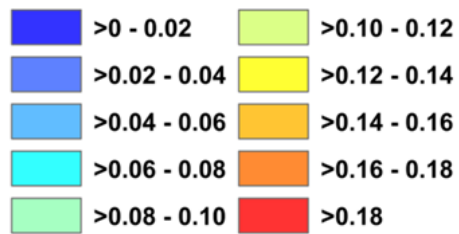


**Figure 7.**



$q'$ : Case 1



$\delta_{q'}$ : Cases 2:4

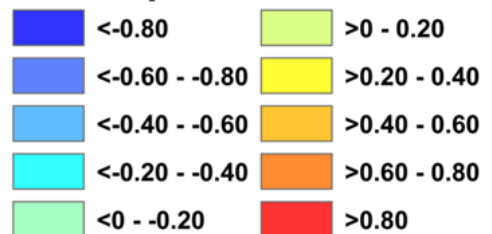
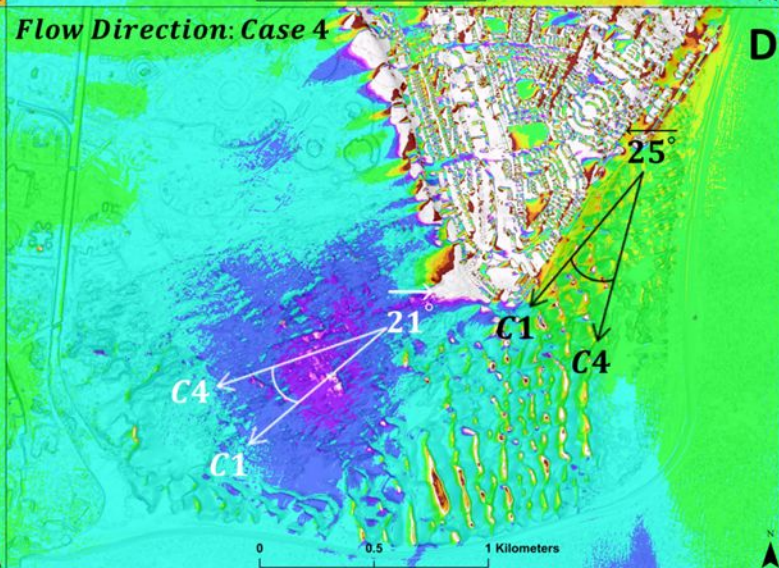
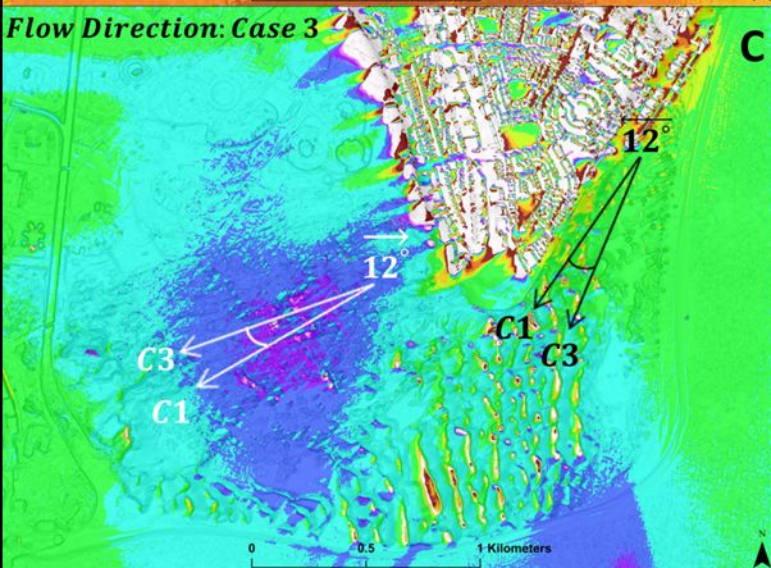
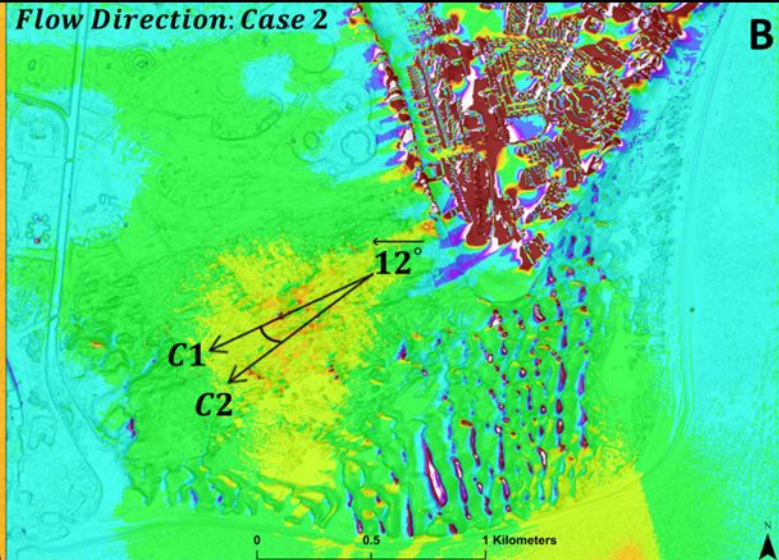
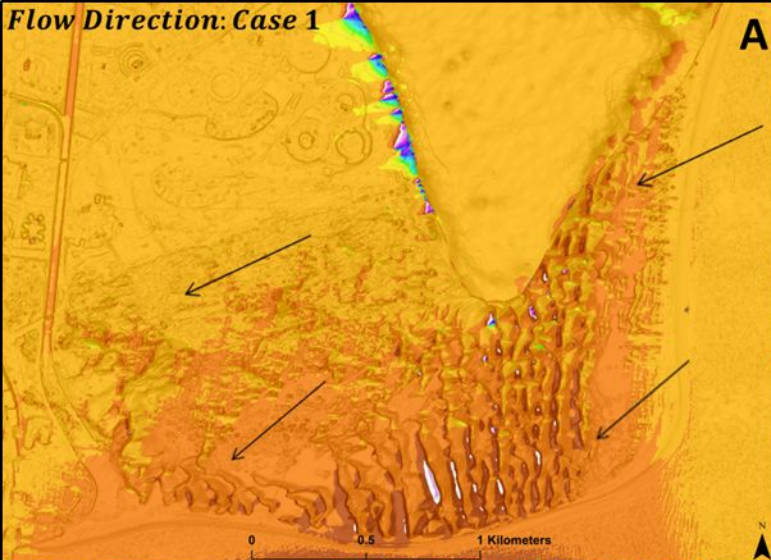


**Figure 8.**



$\theta$ : Case 1



$\Delta\theta$ : Cases 2:4

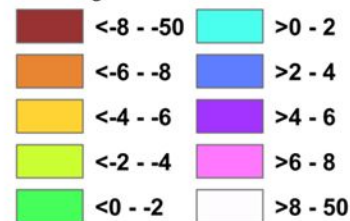
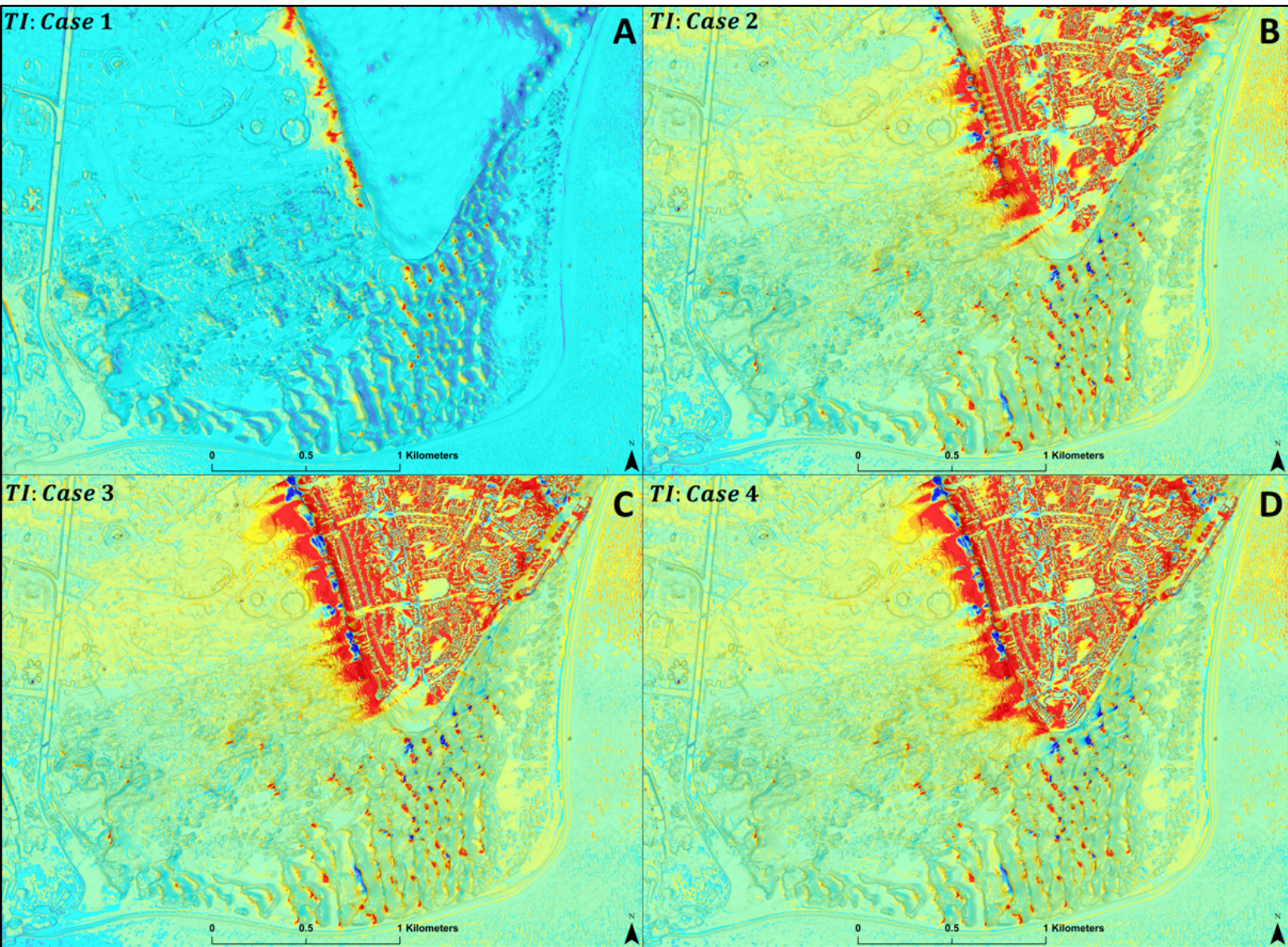
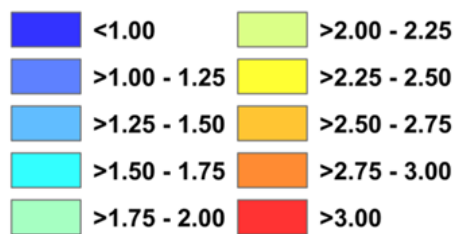




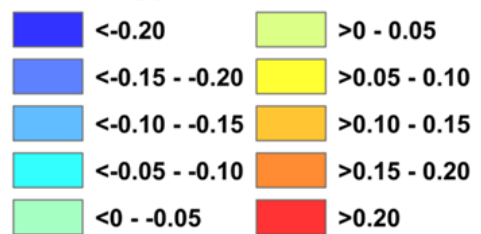
**Figure 9.**



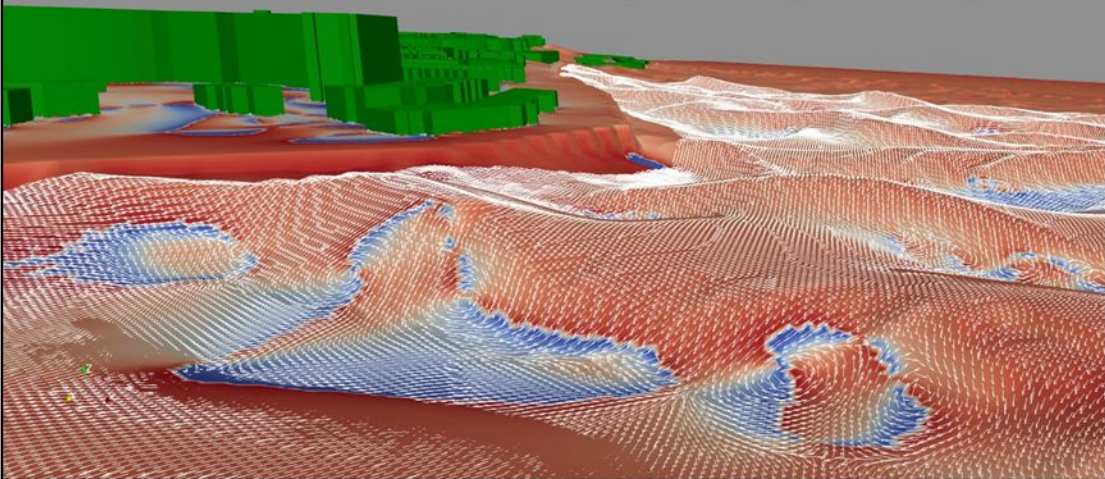
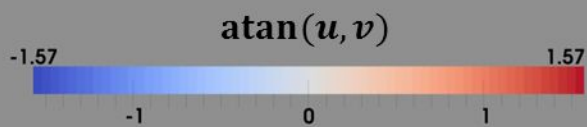
***TI: Case 1***



***$\delta_{TI}$ : Cases 2:4***



**Figure 10.**

**A****B**

$\text{atan}(u, v)$

